Article

Current Biology

Distributed cell assemblies spanning prefrontal cortex and striatum

Highlights

- Neurons fire at high synchrony (~10 ms) in prefrontal-striatal assemblies
- For assembly activations, members phase lock to 4 and 8 Hz rhythms
- Behavioral correlates are more robustly expressed by assemblies than their members
- The assemblies are endogenously generated, spontaneously reactivating during rest

Authors

Virginie J. Oberto, Céline J. Boucly, HongYing Gao, Ralitsa Todorova, Michaël B. Zugaro, Sidney I. Wiener

Correspondence

sidney.wiener@college-de-france.fr

In brief

Synchronous co-activations foster communication in cortical networks. Oberto et al. show very tight synchrony of prefrontal cortical and subcortical (striatal) neurons, coordinated by slow and fast brain rhythms. This leads to emergence of executive function-related behavioral correlates more robust than those expressed by the individual neurons.

Oberto et al., 2022, Current Biology *32*, 1–13
January 10, 2022
https://doi.org/10.1016/j.cub.2021.10.007

CellPress

Current Biology

CellPress
OPEN ACCESS

Article

Distributed cell assemblies spanning prefrontal cortex and striatum

Virginie J. Oberto,[1,2] Céline J. Boucly,[1,2] HongYing Gao,[1,2] Ralitsa Todorova,[1] Michaël B. Zugaro,[1] and Sidney I. Wiener[1,3,*]

[1]Center for Interdisciplinary Research in Biology (CIRB), College de France, CNRS, INSERM, Université PSL, Paris, France
[2]These authors contributed equally
[3]Lead contact
*Correspondence: sidney.wiener@college-de-france.fr
https://doi.org/10.1016/j.cub.2021.10.007

SUMMARY

Highly synchronous neuronal assembly activity is deemed essential for cognitive brain function. In theory, such synchrony could coordinate multiple brain areas performing complementary processes. However, cell assemblies have been observed only in single structures, typically cortical areas, and little is known about their synchrony with downstream subcortical structures, such as the striatum. Here, we demonstrate distributed cell assemblies activated at high synchrony (~10 ms) spanning prefrontal cortex and striatum. In addition to including neurons at different brain hierarchical levels, surprisingly, they synchronized functionally distinct limbic and associative sub-regions. These assembly activations occurred when members shifted their firing phase relative to ongoing 4 Hz and theta rhythms, in association with high gamma oscillations. This suggests that these rhythms could mediate the emergence of cross-structural assemblies. To test for the role of assemblies in behavior, we trained the rats to perform a task requiring cognitive flexibility, alternating between two different rules in a T-maze. Overall, assembly activations were correlated with task-relevant parameters, including impending choice, reward, rule, or rule order. Moreover, these behavioral correlates were more robustly expressed by assemblies than by their individual member neurons. Finally, to verify whether assemblies can be endogenously generated, we found that they were indeed spontaneously reactivated during sleep and quiet immobility. Thus, cell assemblies are a more general coding mechanism than previously envisioned, linking distributed neocortical and subcortical areas at high synchrony.

INTRODUCTION

Complex brain functions have long been proposed to be mediated by the concerted action of groups of neurons ("cell assemblies").[1,2] Yet experimental evidence for this remains scarce. While coordinated neuronal firing has been reported in some cortical areas (see, e.g., Harris et al.,[3] Uhlhaas et al.,[4] and Peyrache et al.[5]), this has more rarely been observed in subcortical areas.[6–8] Further, the reported timescales of coordination have generally been one or two orders of magnitude above those required for neuronal communication or plasticity mechanisms (e.g., post-synaptic membrane time constants[9] or spike-timing-dependent plasticity rules),[10,11] limiting their functional relevance. Conversely, there is little evidence for co-activation at such a fast (~10 ms) timescale or for distributed synchrony, i.e., multi-neuronal assemblies spanning multiple cortical areas (e.g., for sensorimotor processing).[12,13]

One system to study distributed synchrony in cortical-subcortical areas is the cortico-striatal pathway, which is composed of multiple parallel loops for sensorimotor, associative, and limbic processing. The latter includes monosynaptic projections from rat medial prefrontal cortex (PFC) to ventral and medial striatum (STR), which projects polysynaptically back to PFC. This is of particular interest because of this pathway's role in executive processes, such as adapting behavioral response policies in goal-directed behavior, and as an interface between limbic and motor systems.[14]

The convergence and overlap of striatal inputs from multiple cortical areas[15] raises the question of whether and how precisely cortical and striatal neurons can be synchronized while integrating information across hierarchical and functional territories.[16] While cortical-subcortical pairs of neurons fire synchronously (archicortex: hippocampus-ventral striatum;[17] hippocampus-lateral septum;[18] periallocortex: retrosplenial cortex-anterodorsal thalamic nucleus)[19] and hippocampal and striatal assemblies are sequentially activated,[7] precise synchrony has not been observed in large distributed assemblies spanning neocortex and striatum.

One potential mechanism for achieving precise temporal coordination in distributed cell assemblies is phase-locking to oscillations of brain activity.[20] Indeed, previous studies have shown that neurons are synchronized to regular rhythms within PFC or STR (reviews: Pennartz et al.,[21] Benchenane et al.,[22] and van der Meer et al.[23]). Synchrony at low frequencies like 4 Hz and theta has been found among hippocampus, prefrontal cortex, amygdala, and striatum pathways.[24–30] But such studies in the cortico-striatal pathway have largely focused on the sensorimotor loop encompassing dorsolateral striatum

(e.g., Weineck et al.,[31] Antzoulatos and Miller,[32] Koralek et al.,[33] and Donnelly et al.[34]) and have never been shown to be associated with synchronizing cross-structural assembly activity. Thus, it is of interest to characterize synchrony in the associative and limbic prefrontal pathways in the context of their respective roles for cognitive flexibility in goal-directed decision making.

Here, we demonstrate that groups of PFC and STR neurons fire synchronously at high precision. Surprisingly, these cell assemblies integrate neuronal activity from dorsal and ventral sub-regions of both PFC and STR, which have generally been considered functionally distinct. Assemblies emerged as individual neurons shifted their preferred phase relative to ongoing rhythms. They had robust behavioral correlates that appeared only to some extent in their members. Finally, assemblies reactivated during sleep and quiet immobility, indicating that they were endogenously generated and not simply driven by behavioral events.

RESULTS

Neocortical and subcortical neurons form cross-structural assemblies

We performed large-scale simultaneous recordings in medial PFC and downstream dorsomedial and ventral STR neurons (Figure S1A; Table S1) of rats performing a task designed to engage these structures.[35–39] To test for coordinated activity between PFC and STR, we first performed a combined principal- and independent-component analysis (PCA-ICA) from data recorded during awake behavior. This identified numerous stereotyped spiking patterns spanning both structures at a timescale consistent with cross-structural communication (Figures 1A and 1B; Table S2). To quantify this timescale, we systematically varied the time windows analyzed. Unexpectedly, most (70%) of these motifs persisted for time windows as brief as 10 ms (Figures S1B–S1F), indicating that they formed cell assemblies.[3]

Of the 74 detected assemblies (containing 2–16 members; mean = 6.8 ± 3.1 cells; Table S2), almost half were neocortical-subcortical, spanning both STR and PFC (“STR+PFC”; n = 32; e.g., Figure 1A, assemblies 1 and 3). While the remaining half were detected in only a single structure (“STR only,” n = 33; Figure 1A, assembly 4; “PFC only,” n = 9; Figure 1A, assembly 2), this generally occurred when only one or two neurons were recorded in the other structure (Table S2), suggesting that most assemblies might actually span both structures.

Another unforeseen result was that, in almost all sessions, assemblies included neurons of functionally distinct sub-regions of both PFC and STR (83% of sessions for dorsomedial and ventral STR, Figure 1A, assembly 4; 85% of sessions for dPFC and vPFC, Figure 1A, assembly 2; tallied for sessions with three or more neurons in each structure).

To more precisely characterize the timescale of the synchrony, we cross-correlated spikes of PFC-STR neuron pairs. STR spiking was significantly elevated in a [−15, 30] ms window around PFC spikes (shaded gray area in Figure 1C, left). The cross-correlograms were significantly asymmetric (median asymmetry index = 0.1; Wilcoxon sign rank test $p = 6.9e{-}27$), consistent with PFC neurons driving STR neurons during assembly activations. This is not a general property of all PFC-STR pairs because we did not detect any significant peak in cross-correlations between pairs of PFC and STR neurons that were not members of the same assemblies (Figure 1C, right; the non-significant bump at zero could be due to pairs belonging to under-sampled and hence undetected assemblies).

Assemblies emerge as member neurons shift phase to align with brain rhythms

Prefrontal assemblies form during bouts of synchronous theta oscillations in hippocampus and PFC,[27] suggesting that distributed PFC-STR assemblies could also emerge from phase realignment with ongoing rhythms.[20] In a T-maze task, as shown previously, two principal bands dominated the LFPs: 4 Hz and theta (8 Hz; Figures 2A and 2B, right columns). Consistent with synchronization of cells by oscillatory rhythms (Figure S2C), nearly half of the assemblies were phase-locked to 4 Hz (∼40%) or theta (∼50%; Figures 2D and 2E; assembly activation time was taken as the peak in activation strength; cf. Figure 1B). Modulation by at least one of these rhythms occurred in most assemblies with members in different sub-regions (dPFC+vPFC, 67%; dmSTR+vSTR, 59%) or STR+PFC (64%). Notably, oscillatory power and coherence were significantly elevated on delimited segments of the maze that elicited distinct behaviors and cognitive processes (on the central arm for 4 Hz but on return arms for theta; Figures 2A, 2B, and S2B). A Granger analysis revealed that PFC oscillations led STR at both 4 Hz and theta (Figure 2C), again consistent with the uni-directionality of monosynaptic PFC-STR projections (although, alternatively, PFC and STR could receive common but delayed driving inputs). All analyses below refer to PFC oscillations.

To investigate whether assembly activations were dynamically associated with phase-locking of individual members, oscillatory cycles containing assembly activations (“IN”) were compared to all other cycles (“OUT”) for both 4 Hz and theta. As predicted, substantially more assembly members were phase- locked to 4 Hz and theta during IN cycles (Figure 2F; except for interneurons at 4 Hz). An independent analysis based on pairwise phase consistency replicated this (Figure S2D). As expected, during IN cycles, both STR and PFC principal neuron members were phase locked to the average preferred phase of the assemblies (compare Figures 2E and 2G), but this was not the case for OUT cycles (Figure 2G; downsampling the number of data points to balance them across conditions yielded the same results; Figure S2F). Thus, on average, principal neurons shifted their preferred phase to the overall mean phase of assembly activation. We further tested whether members shifted to the phase of their respective assemblies, even when taking into account variations in the latter’s preferred phases. While this did occur for principal neurons of both STR and PFC, for both 4 Hz and theta (Figure 2H), interneurons, on the other hand, remained at the assemblies’ preferred phases during both IN and OUT cycles (Figure 2H). This was not due to restricting analyses only to phase-locked members: the same result was obtained using all assembly members (Figure S2E). Overall, this suggests that entrainment of principal neurons to a common preferred phase is crucial for assembly formation.

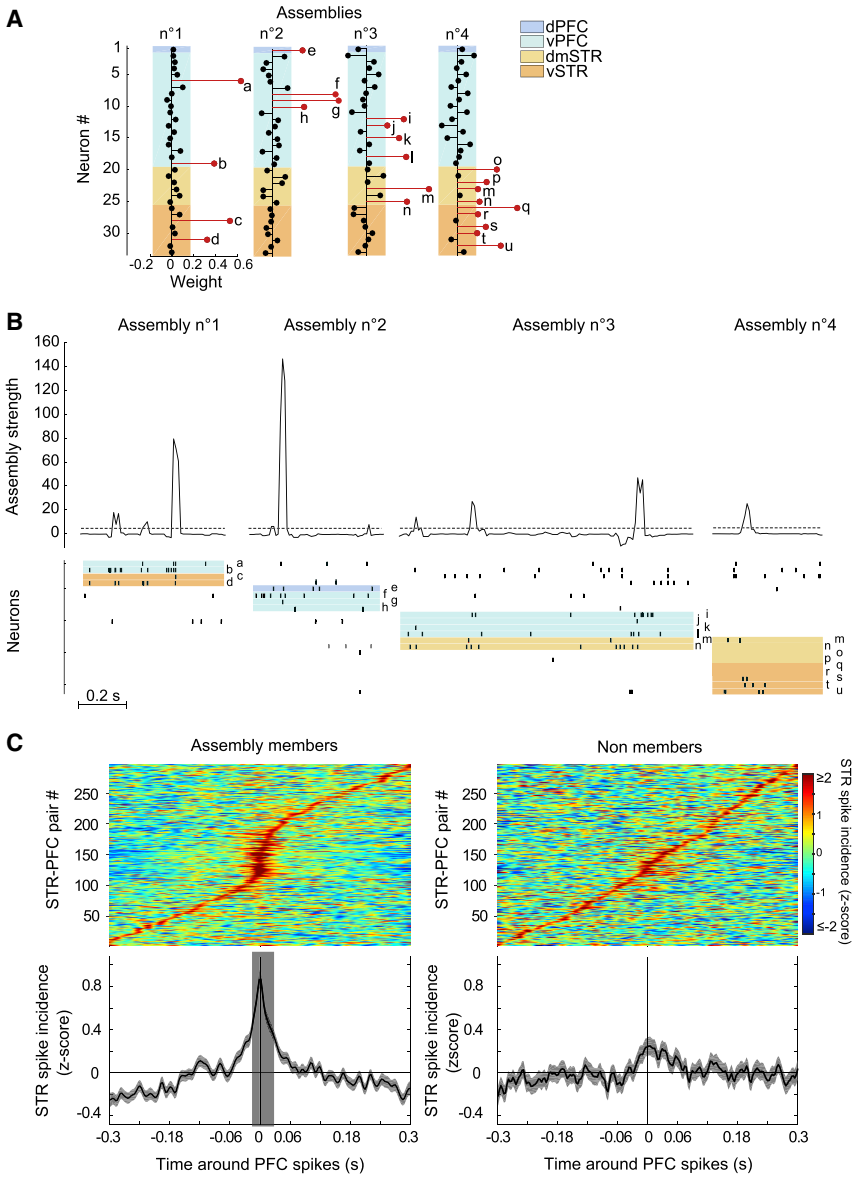

Figure 1. Assemblies of STR and PFC neurons

(A) Four assemblies exceeding the Marčenko-Pastur threshold (cf. Figure S1B) in a representative session (corresponding to session 10, assemblies 42, 43, 44, and 46 in Table S2). Assembly "members" (red "lollipops") exceeded the ICA weight threshold (abs(1/√N): lateral edges of colored bars. Infralimbic and prelimbic cortex (IL and PL) are grouped together as "vPFC" while cingulate cortex (Cg1) is labeled "dPFC." Core and shell zones of the nucleus accumbens are grouped together as "vSTR." dmSTR is dorsomedial striatum.

(B) Examples of assembly activations. Cells are identified by letters (re-ordered from A to highlight the respective assemblies). Note that multiple neurons fire during assembly activations—in the dataset, approximately half of all assembly activations involved three or more neurons. The dashed horizontal lines indicate the activation strength threshold. Color code and identifying letters are the same as in (A).

(C) Cross-correlations of STR-PFC cell pairs from all cross-structural assemblies. Top: color plots ordered by the onset of the peak *Z* score value (3 ms bins) are shown. Bottom: averages of the above data are shown (mean ± SEM; shaded bar: $p < 0.05$, Monte-Carlo bootstrap). The bin width selected for assembly detection here was 30 ms (cf. Figure S1F). Left: all neuron pairs that were both members of the same assembly are shown. Right: cross-correlograms of randomly selected pairs of neurons that were not members of the same assemblies are shown.

See Figure S1 and Tables S1 and S2.

Both 4 Hz and theta rhythms modulated gamma oscillations in STR (Figure 3A),[26,34] which in turn could help govern precise synchrony among PFC and STR neurons. Several frequency bands were modulated by 4 Hz and theta oscillations, but only "gamma-80" (70–100 Hz) was modulated at a phase near that of the assemblies (near 2π; cf. Figures 2E and 3A). In order to test for possible association with assembly member synchronization, this band was selected for further analysis. Assembly activations were more frequent during gamma-80 bursts (Figure 3C), and reciprocally, in cycles containing assembly activations, there were more gamma-80 bursts (Figure S2G; and higher gamma-80 power; Friedman tests; $p < 0.05$). More precisely, 4 Hz and theta phase-locked assembly activations tightly synchronized with the onsets of gamma burst (Figures 3B and S2A), but this was not the case for assemblies with no phase-locking. This is consistent with the hypothesis that gamma-80 onset facilitates assembly member synchrony.

Gamma-80 phase locking of PFC principal neuron members differed from that of STR principal neuron members by a quarter of a cycle (corresponding to ~3 ms; Figure 3D), consistent with tight coupling, and on the order of the timescale of the PFC to STR conduction time.[40,41] Figure 3E summarizes the timing of assembly activation relative to 4 Hz, theta, and gamma-80. This illustrates the realignment of principal neurons (but not interneurons) to the assembly activations at the beginning of gamma bursts and at specific phases of 4 Hz and theta cycles.

Functional correlates in neocortico-striatal assemblies

Cell assemblies are hypothesized to underlie brain computations and even cognitive functions, possibly extending beyond such processing by their individual members. We thus investigated the functional correlates of the cross-structural assemblies. In a flexible decision-making T-maze task (Figure 4A), 31% of the 74 assemblies were preferentially activated on limited segments of the maze, respectively corresponding to different behavioral and cognitive aspects of the task (Figures 4D–4F, top row, 4G, and 4J; referred to as "spatial" selectivity), such as decision-making and reward approach. These spatial correlates were often modulated by other task-relevant behavioral factors,

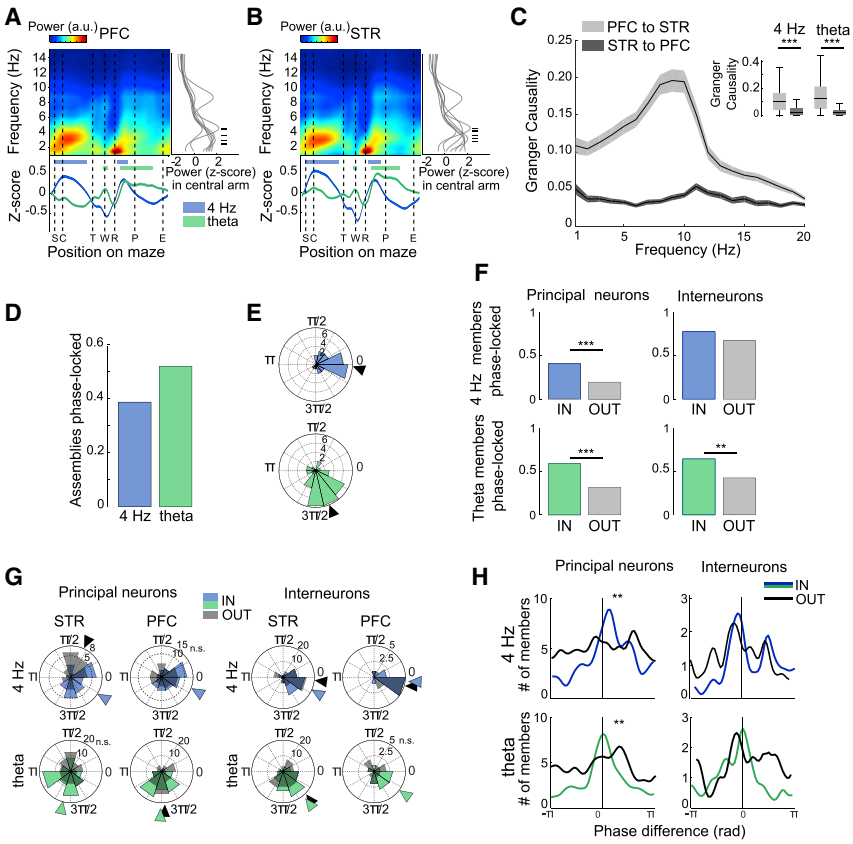

Figure 2. Assemblies and their members phase lock to 4 Hz and theta oscillations

(A and B) Mean spectrogram (top) and 4 Hz and theta power distributions (below) on a linearized projection of the maze (S, start point; C, cue onset; T, turn; W, reward photodetector; R, reward site; P, cue off; E, trial end; cf. Figure 4A). Horizontal color-coded bars indicate maze segments with significantly higher Z scores ($p < 0.05$; Monte Carlo bootstrap). Both the color and the Z score scales are linear. Right: average power of the spectrograms for each rat (gray traces) and overall average (black trace) from data recorded in the central arm are shown. Hashmarks show modes for the respective rats. a.u., arbitrary units.

(C) Average spectral Granger causality between PFC and STR LFPs (mean ± SEM). Inset compares the two directional values for 4 Hz (Wilcoxon sign-rank test: $p = 1.9e{-}79$) and 8 Hz ($p = 9.8e{-}77$; $n = 20$ sessions for each). Horizontal bars represent the median, boxes indicate the 25th and 75th percentiles, and whiskers are minimum and maximum values.

(D) Proportions of assemblies phase-locked to 4 Hz and theta bands (n = 74 assemblies).

(E) Distribution of the mean phases for all assemblies significantly phase-locked to PFC 4 Hz or theta oscillations. Arrowheads indicate the distribution means. For assemblies phase-locked to 4 Hz, Rayleigh test: mean angle m = 0 rad, $p = 7.2e{-}06$; for theta, Rayleigh test: $m = -1.3$, $p = 1.3e{-}06$.

(F) Proportions of principal and interneuron members phase-locked during oscillation cycles with assembly activations (IN) and those without (OUT; binomial tests: 4 Hz $p = 1.0e{-}04$ and 0.17; theta $p = 9.7e{-}08$ and $3.8e{-}03$, respectively).

(G) Distributions of the mean phases of phase-locked members IN (color) and OUT (gray). Arrowheads mark significant distribution means (Rayleigh test: $p < 0.05$).

(H) Distribution of the differences between mean phase angle of each assembly (at zero) and the mean for each individual phase-locked member IN (color coded) and OUT (gray). Kuiper test (comparison of two circular distributions): 4 Hz $p = 0.001$ and 1; theta $p = 0.002$ and 1, respectively, for principal neurons and interneurons.

See Figure S2 and Table S3.

such as left versus right choices (“side” selectivity) or rewarded versus non-rewarded choices (“rewarded”; Figures 4J and S3).

The rats alternated between two goal-directed tasks in the T-maze (Figure 4A). The animals first performed a visual discrimination task (VD1), then a spatial discrimination (SD), and finally the same visual task again with the same cue contingency (VD2; Figures 4B and 4C). Assemblies were selective for “task conditions” (VD1, SD, and VD2; Figures 4E and 4F). Interestingly, more assemblies discriminated between repetitions of the same task (VD1 versus VD2) than between different tasks (SD versus VD1 or SD versus VD2; Figures 4E, 4F, and 4I), and these were distinctly distributed on the maze (Figure 4H). This is consistent with population analyses of PFC neurons[42] and is extended here to PFC-STR assemblies. This persisted after correction for linear drift in firing rates (which could accompany decreased motivation along the course of the session) or behavioral parameters, such as reward arm choice, speed, or vicarious trial and error behavior (STAR Methods; Figure S4).

To assess whether behavioral correlates of assemblies merely derived from those of their members or whether more complex integration took place, we first characterized the selectivity of individual members. Substantial proportions of individual STR and PFC neurons fired selectively for several trial characteristics, including reward arm choice (left or right), reward outcome (Figures 5C and S3), and between-task conditions (Figures 5A–5C and S5). Among the three task condition comparisons, VD1 versus VD2 firing rate differences were predominant but only in STR neurons (Figure 5B). Firing rate differences between task conditions were differentially distributed on the maze (Figures S5 and 5A; corrected for linear drift, Figures S4B–S4D), and a support vector machine model (SVM) trained on STR population activity reliably classified the ongoing task conditions, including VD1 versus VD2 (Figure 5D; also for PFC, Wilcoxon signed-rank tests; $p = 0.039$, 0.043, and 0.034, respectively).

Emergence or overlap of member behavioral correlates in their assemblies

In many cases, the behavioral correlates of assemblies resembled those of their members in the same part of the maze (e.g., Figure 6A; black bars in Figure 6C), and this was more prevalent than found after random reassignment of members’ significant correlates (Figure S6C). However, on the other hand, we often observed differences between significant behavioral correlates of assemblies and members, consistent with our hypothesis

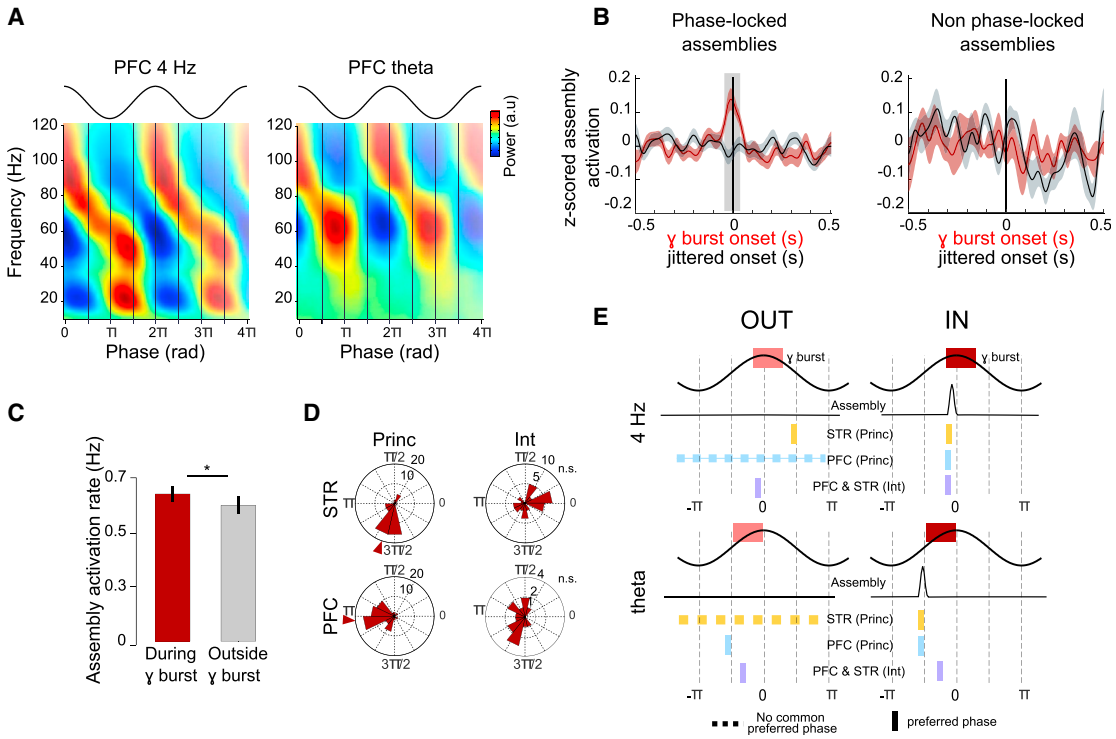

Figure 3. Gamma-80 oscillations and synchrony

(A) Average PFC 4-Hz and theta LFP modulation of higher frequency bands of PFC LFPs (n = 20 sessions).

(B) Mean (traces) and SEM (shading) of *Z* scored PETHs of assembly activations triggered at the onset of gamma-80 bursts for assemblies phase-locked to 4 Hz and/or theta (left; n = 52) and others with no 4 Hz or theta phase-locking (right; n = 22; red: centered on gamma bursts; black: centered on randomly jittered gamma bursts onset times; mean ± SEM; shaded vertical bar: $p < 0.05$, Monte-Carlo bootstrap). Also see Figure S2G.

(C) Activation of assemblies is greater within than outside of gamma-80 bursts (mean ± SEM; Wilcoxon signed-rank test; $p = 0.043$; n = 74 assemblies).

(D) Distributions and preferred angles of phase-locking to PFC gamma-80 in all STR and PFC principal neuron and interneuron members. Arrowheads indicate significant mean angles (n.s., not significant).

(E) Summary of alignments of the respective phase relations OUT versus IN for 4 Hz and theta. Int, interneurons; Princ, principal neurons.

See Figure S2 and Table S3.

that the former are not simply a reflection of the latter. Indeed, members could be selective where assemblies were not ("filtering," e.g., Figure 6B, assemblies 29, 35, and 45). Moreover, we observed evidence of emergent properties, where the assemblies were significantly selective for behavioral correlates even though the members were not (e.g., Figure 6B). This occurred in 29% of assemblies with left versus right (side) choice correlates, 75% with reward correlates, and 41% with task order correlates (white bars in Figure 6C). Behavioral correlates were more strongly expressed in assemblies than their members (Figure 6D), providing further evidence for emergent properties. Interestingly, within the same assembly, members could have overlap for some behavioral correlates, but there could be filtering and/or emergence for others (Figure S6A).

One possible explanation for the emergent properties is that non-significant (according to the Monte Carlo analysis) trends in members could be expressed significantly in their assembly's behavioral correlate (e.g., in Figure 6B, note black curves in lower plots for assemblies 14 and 45). To test this, we searched for non-significant trends in members corresponding to their assembly's behavioral correlates. For this, we measured their respective differences in firing rates for trial characteristics (e.g., in trials with left versus right side choices) at the maze positions of their assembly's behaviorally correlated activity. As a control, we measured differences in these neurons' firing rates for trial characteristics at randomly selected locations on the maze. The pooled distributions of these differences are plotted for all behavioral correlates in Figure 6E, and they are significantly different (see Figure S6B for the respective behavioral correlates). Next, we tested whether assembly emergent properties could arise when non-significant trends in members were weak or stronger trends. Indeed, in numerous cases, assembly correlates emerged even when the peak firing (at the same location as the assembly) of non-significant members was inferior to the (arbitrary) criterion of 1.5 z (white bars in Figure S6D). Altogether, this supports the hypothesis that cell assemblies have emergent properties, bringing forth behavioral correlates reflecting non-significant tendencies in their individual members.

Prefrontal-striatal assemblies can be internally generated

These analyses indicate that synchronous activity among neurons did not simply result from common inputs triggered by behavioral events (because, for instance, the same sensory and motor processes triggered different assembly activation rates in VD1 versus VD2). Yet a more direct proof would be to show that distributed

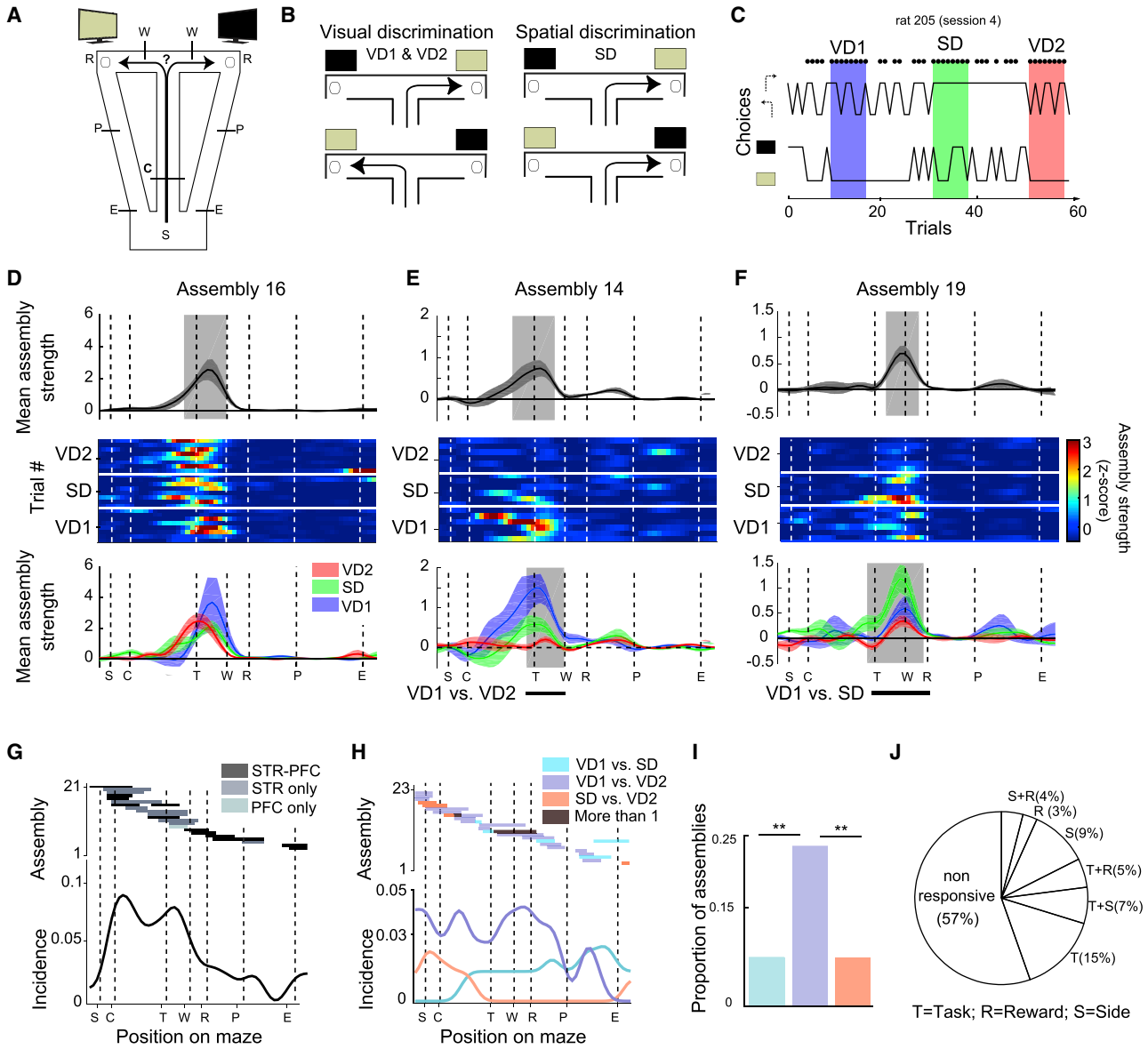

Figure 4. STR-PFC assembly activations are behaviorally selective

(A) In this completely automated T-maze, rats self-initiated trials by crossing a photo-detector C near the beginning of the central arm to trigger visual cues (in pseudo-random sequence) on two TV screens behind the reward arms. Following correct choices, a photo-detector, W, on the reward arm triggered release of a sweetened liquid reward at a reward site R. S, trial start point; P, photo-detectors triggering cues off; E, trial end point.

(B) In the VD task, the screens indicated the rewarded arm, while in SD, the rat's non-preferred arm (right or left) was rewarded, irrespective of the cue screens.

(C) Behavioral responses during a representative session. Dots above indicate rewarded trials. The upper and lower traces track performance for the SD or VD contingencies. Color-shaded zones indicate criterion performance trials. The rule was changed after criterion performance was reached.

(D–F) Example assembly activations on a linearized projection of the maze. Top row: mean (traces) and SEM (shading) of activation strengths over the entire session are shown. Significant deviations from baseline are marked by light-gray-shaded rectangles ($p < 0.05$; Monte-Carlo bootstrap). Middle row: *Z* scored assembly activation strengths for each trial during the three task conditions are shown. Bottom row: mean (±SEM) assembly activation strengths in the respective task conditions are shown (Monte Carlo bootstrap; $p < 0.0166$; D–F correspond, respectively, to sessions 5, 4, and 4, assemblies 14, 16, and 19; cf., Table S2).

(D) An assembly active during reward arm selection but with no significant differences between task conditions.

(E) A task-order selective assembly (shaded region indicates where activity was higher during VD1 than VD2).

(F) An assembly selective for the SD rule (versus VD1 and VD2).

(G) Distribution of assembly selectivity for maze segments (horizontal bars; Monte Carlo bootstrap $p < 0.05$). Bottom: summary histogram is shown. Incidence is the proportion of assemblies selective for each spatial bin relative to all assemblies (n = 74).

(H) Same as (G) for maze distribution of task condition selectivity of assemblies.

(legend continued on next page)

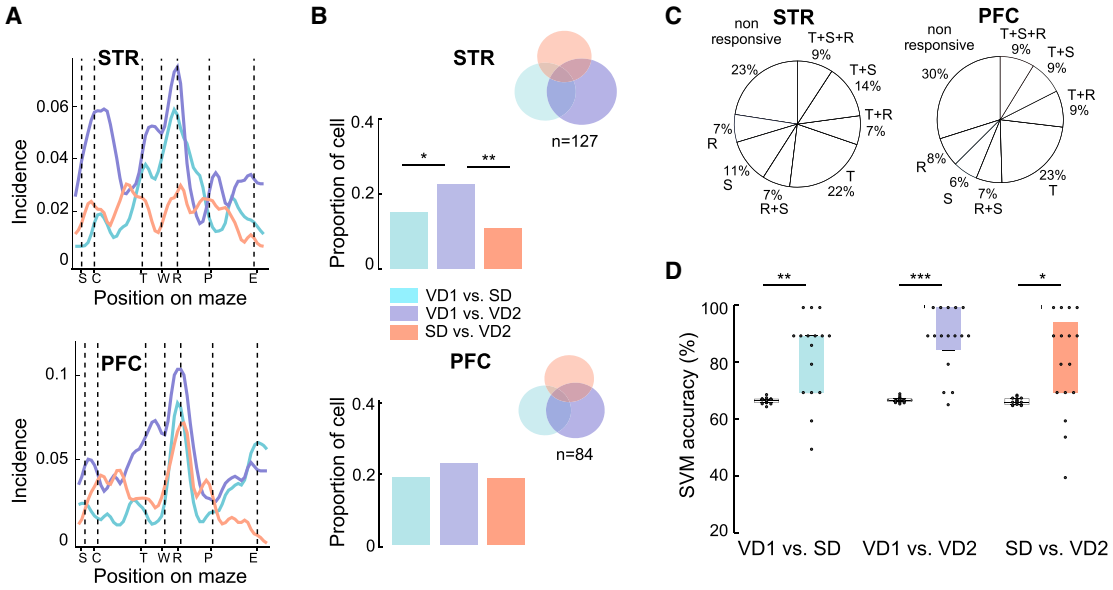

Figure 5. Behavioral correlates of STR and PFC neurons

(A) Distributions of significant task condition differences of single neurons along the linearized maze (cf. Figure S5 for details). Incidence is the fraction of cells selective for each spatial bin relative to all recorded cells (n = 295 for STR and n = 185 for PFC).

(B) Proportions of cells selective for each task condition comparison (binomial tests: p = 0.02, 0.13, and 2.1e−4 and p = 0.31, 0.79, and 0.20, respectively, for STR [n = 295] and PFC [n = 185]). Upper right: proportions of cells (areas of circles) selective for single and multiple task condition comparisons are shown.

(C) Behavioral correlates (same abbreviations as Figure 4J).

(D) Support vector machine models trained on STR population activity successfully classify task conditions. The SVM prediction accuracies (color-coded boxplots extend from 25% to 75% quartiles) are significantly higher than those for randomized datasets (white boxplots to the left; Wilcoxon signed-rank test: VD1 versus SD, p = 0.0027; VD2 versus SD, p = 0.02; VD1 versus VD2, p = 0.0008; n = 16 sessions). Each point represents one session.

See Figures S3–S5.

assemblies also activate in the absence of behavioral events. We thus tested for endogenous assembly reactivation during the post-task "sleep session" in a flowerpot (which also included quiet immobility but no task-related cues or behaviors). Not only did we find assembly reactivation, but in addition, PFC-STR assembly activity was significantly higher during the post-task sleep session than during the pre-task sleep session (Figure 6F), similar to observations in hippocampal-accumbens cell pairs.[17] In individual assemblies, activation rates of 34% of the assemblies significantly increased during post-task sleep relative to pre-task sleep sessions, although they decreased in 8% (binomial comparison, $p < 0.05$; cf. Table S2). Because reactivation of neural patterns of activity during sleep and quiet immobility, including recordings in PFC and vSTR, has been linked with memory consolidation,[17,43,44] this suggests that distributed assemblies could participate in offline memory consolidation.

DISCUSSION

Here, we showed highly synchronous neuronal assemblies in medial PFC and limbic and associative STR. Not only did these assemblies unexpectedly include members from hierarchically distinct brain areas (cortex versus non-cortex), but they also integrated members from functionally diverse and reportedly distinct loops in the cortico-striatal pathway. Assemblies emerged when spikes of principal neurons shifted in phase relative to 4 Hz and/or theta rhythms and were accompanied by increased gamma activity. Assembly activations were associated with specific behavioral parameters of a set-shifting task. In many cases, assemblies represented non-significant firing trends of individual members, bringing forth significant behavioral correlates. Finally, assemblies were selectively reactivated during sleep and quiet immobility after behavioral sessions, indicating that they were independent of specific behavioral inputs and that they could be involved in memory consolidation processes.

Distributed assemblies coordinate functionally distinct sub-regions at a precise timescale

Previous studies have documented cell assemblies confined to a single structure (e.g., PFC,[5,45] STR,[8] and also for STR cell pairs),[46,47] and assemblies detected independently in PFC and STR activate sequentially.[7] Synchronous cortico-subcortical

(I) Proportions of assemblies showing the three types of task condition selectivity (binomial tests: p = 0.0056, 0.0056, and 1, respectively; n = 74 assemblies; cf. Table S2).

(J) Proportions of assemblies selective for different task conditions (T) on rewarded versus unrewarded trials (R) and/or on leftward versus rightward trials (S). See Figure S3.

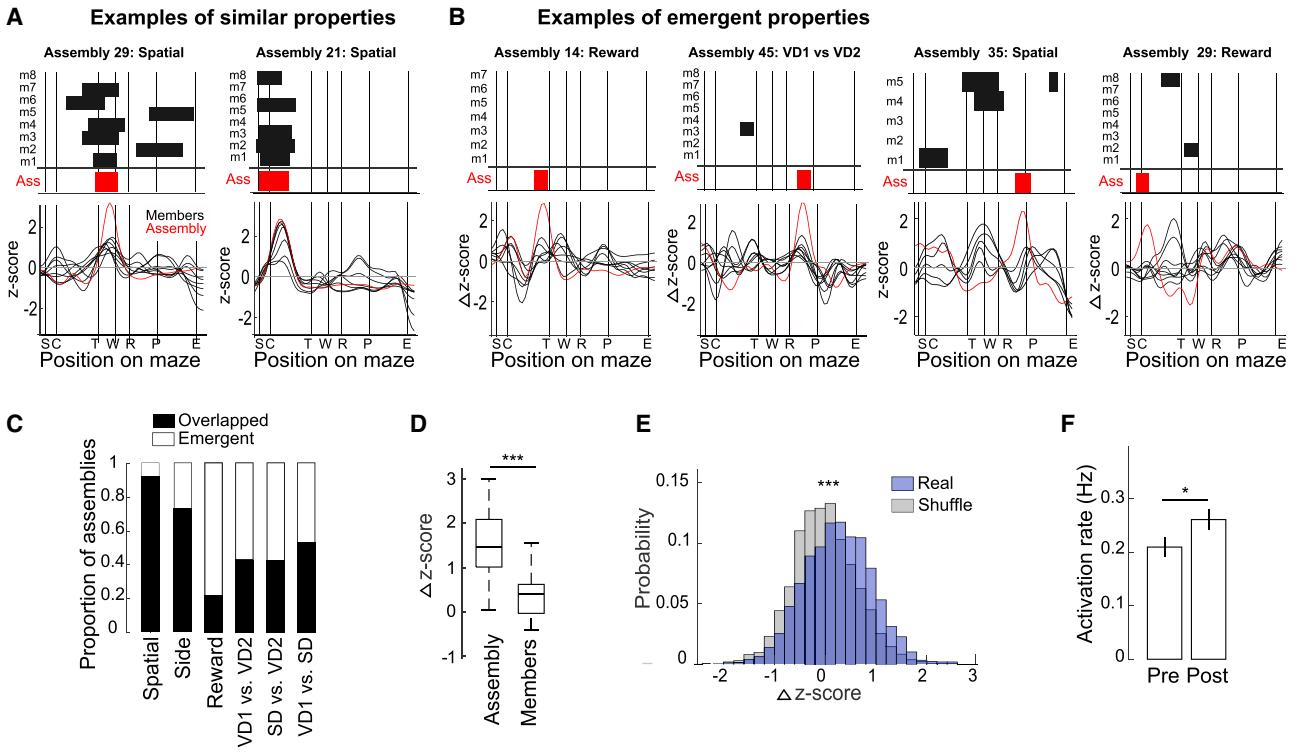

Figure 6. Similarities and differences in behavioral correlates of assemblies and their members

(A and B) Comparison of behavioral correlates of representative assemblies (Ass) and their members (mX). Top: areas on the maze where the assembly (red) and its members (black) had significant behaviorally correlated activity (indicated by bars, as in upper plots of Figures 4G and 4H; Monte Carlo bootstrap; $p < 0.0166$ for task condition and $p < 0.05$ for all others. The absence of bars indicates that tests were not significant.). Bottom: Z scored differences in assembly activation rates (red curve) or members' firing rates (black curves) between the respective pairs of trial types are shown (e.g., for reward: rewarded minus unrewarded trials). For "spatial," the *Z* score is for selective activation at positions on the maze.

(A) Significant correlates of respective assemblies and their members are in overlapping maze locations.

(B) Assembly activations are significant while those of members are not.

(C) Proportion of assemblies with behavioral correlates overlapping with at least one member (black bar) or emergence of significant behavioral correlates not present in their members (white bar). Respective n's are 21, 14, 8, 17, 5, and 5.

(D) Comparison of the *Z* scored trial characteristic differences between assembly activity versus firing rate differences of their members at locations where their assembly shows emergent properties (plots as in Figure 2C; Wilcoxon signed-rank test: $p = 3e{-}09$).

(E) Actual ("real") distribution of firing rate differences of the members for all behavioral correlates pooled together at locations where their assembly's activation was significant, but members were not, and the distribution of these measures for the same cells but at randomly assigned locations ("shuffle"). Positive *Z* scores signify that activity changes of members are consistent with those of the assembly (Wilcoxon signed-rank test: $p = 6.3e{-}46$).

(F) Assembly activation rate was greater during post-task (post) than pre-task (pre) sleep (Wilcoxon signed-rank test: $p = 1.3e{-}04$; $n = 59$).

Also see Figure S6.

cell pairs have been reported (hippocampus and STR;[6,17,48] retrosplenial cortex and thalamus;[19] hippocampus and septum),[18] and it is often inferred that they are proxies for more widespread synchronization of assemblies. Here, we demonstrate such larger scale synchrony in the prefrontal-striatal pathway for the first time, to our knowledge.

Concerning timescales, recent studies have reported highly synchronous (25 ms) ventral striatal cell assemblies[7,8] and PFC cell assemblies (with 100-ms[5] and 150-ms[49] bins) using PCA-ICA. Long latencies between spikes would not be propitious for coincidence detection in downstream "readers,"[2] where convergent inputs from assemblies must arrive in brief time windows on the order of 8 ms.[50] The cross-structural assemblies here are maintained at this timescale.

Distinct pairs of zones of the cortex and striatum are linked in recurrent loops.[15] Classically, each loop is considered to underlie complementary functions.[16] Here, assemblies bridged STR and PFC sub-regions with markedly distinct functions, ranging from associative learning to goal-directed behavior (e.g., Ito and Doya[51]). Indeed, functional inactivation and metabolic marker studies have revealed different types of processing in sub-regions of STR[38] and PFC.[52,53] The evidence that PFC and STR sub-regions execute distinct functional processes does not preclude the possibility of precisely timed cooperation by these "complementary," or even "competing," structures. Membership in assemblies by neurons from functionally distinct prefrontal and striatal sub-regions could be related to the overlapped interconnections among these areas[15,54] or common inputs (e.g., from hippocampus and dopaminergic nuclei). However, the precise synchrony observed here is surprising because individual cortical neurons widely and sparsely project to many striatal neurons.

Interestingly, assemblies also included interneurons, which could contribute either directly via both local and long-range projections or indirectly by silencing competing assemblies.[55] Indeed, the PFC projection to STR medium spiny neurons is a feedforward loop going through parvalbumin fast-spiking interneurons.[56]

Dynamic processing leading to synchrony in STR

Hebb[1] postulated that strengthening of excitatory synaptic connections among members would help give rise to cell assemblies. This would pose a theoretical conundrum because the vast majority of striatal neurons are inhibitory and have sparse local connectivity,[57] and it would thus be unlikely that cell assemblies could emerge only from local striatal circuit interactions. Instead, consistent with the known anatomical projections,[54] conduction delays,[40] and computational simulations,[58,59] timed prefrontal inputs could leverage synchronous striatal activity and/or oscillatory coherence with striatum for distributed assembly activations. Our data are consistent with PFC monosynaptically driving the STR during assembly activations because of the results of the Granger analysis of oscillations, as well as the asymmetry of the spike pair cross-correlograms, although precisely delayed driving inputs from a third structure cannot be excluded. Indeed, precise spike synchrony is observed even between structures not directly connected.[60]

Brain rhythms may synchronize neocortico-subcortical assemblies

According to the "communication through coherence" hypothesis,[20] cross-structural signaling is facilitated when the respective local oscillations are synchronized, concentrating spike activity into brief temporal windows of downstream excitability, leading to firing there. Indeed, here, assembly members shifted their phase-locking to PFC 4 Hz and theta LFPs, leading to synchronous activations. This has not been shown directly in these cortico-striatal pathways before and is consistent with published observations of LFP coherence, and spike phase modulation, between cortex and dorsal STR (e.g., Weineck et al.,[31] Antzoulatos and Miller,[32] Koralek et al.,[33] and Donnelly et al.[34]). Dopamine influences LFP coherence and cell synchrony (e.g., Benchenane et al.,[27] Sala-Bayo et al.,[61] and Gireesh and Plenz[62]), although there are important differences between striatal functional subregions in neurotransmission and anatomical organization. However, our results indicate that coordination of spike synchrony by brain rhythms appear to be a general coordinating principle throughout STR. One possible concern is that assembly co-activations could be fortuitous events arising from the neurons independently phase locking to the same rhythms, particularly when firing at higher rates should their behavioral correlates overlap. However, the frequency of assembly activations (~0.1 Hz) was far lower than that of possible convergences of these events. Such fortuitous synchrony is also inconsistent with observations that, within the same session, independent assemblies were detected, even though they had overlapping behavioral correlates (e.g., assemblies 14 and 16 in Figures 4D and 4E) and similar preferred phases (Figure 2E). Furthermore, the assemblies were reactivated during sleep and quiet immobility, when these rhythms and behaviors are minor or absent. This is the first study, to our knowledge, that shows the association between rhythmic synchrony and synchronization of neuronal firing to form precisely timed distributed assemblies in a cortico-striatal pathway, and it would be interesting to investigate whether this extends to the dorsolateral sensorimotor STR as well.

Synchrony at low frequencies like 4 Hz and theta has been found in hippocampal-prefrontal, prefrontal-amygdalar, and hippocampo-striatal pathways.[24–30,63] The present results suggest that this coordination could extend beyond these pathways for which the ventral striatum is a hub, in a form of network resonance. Moreover, these dynamics could reflect widespread synchrony throughout this extended distributed network,[64] with highly synchronous cell assemblies distributed across these structures.

This dynamic coordination likely extends to humans because synchrony at low frequencies like 4 Hz and theta has been found at multiple levels in the prefrontal cortical-basal ganglia loop (e.g., in human 2–10 Hz).[65,66] Medial prefrontal cortex is in synchrony with ventral STR in human scalp electroencephalograms (EEGs) during reward anticipation.[67] And there is 4 Hz coherence between human prefrontal cortex and subthalamic nucleus (downstream of STR).[68] Long-range gamma synchrony is also observed in humans (e.g., Rodriguez et al.[69] and Arnulfo et al.[70]). These could also be involved in executive processing: in quantitative meta-analyses of fMRI experiments in humans, both the ventral striatum and the medial prefrontal cortex were linked to model-based learning.[71]

The 4 Hz and theta rhythms could exert parallel, alternating, and/or interacting influences to orchestrate brain network activity. Indeed, their highest amplitude LFPs were at different parts of the maze (choice point versus post-reward), which are respectively associated with different cognitive processes. For example, 4 Hz has been described in coupling with amygdala, dopaminergic nuclei, and respiratory coordinating signals (e.g., Fujisawa and Buzsáki,[28] Karalis et al.,[72] and Carmichael et al.[73]), while theta rhythms in PFC and STR could be related to hippocampal theta.[27,29,30,74–76] Moreover, during spatial exploration, theta rhythms synchronize the hippocampus and the vSTR, whereas during lever presses, vSTR is dominated by a transient low-frequency rhythm from the neocortex (e.g., Gruber et al.;[77] for human decision-making, Stenner et al.[78] and Horschig et al.[79]). Sensorimotor STR and PFC neurons in dopamine-depleted rats also have phase preferences in delta and theta bands.[80] These results are consistent with "multiplexing,"[81] wherein simultaneous communication is orchestrated by oscillations at different frequency channels. Here, the 4 Hz and theta rhythms recruited partially overlapping sets of distributed assemblies in relation to ongoing behavioral challenges.

Gamma synchrony

Distributed synchrony of cell activation is suggested by coordinated cortical and striatal oscillations, particularly at gamma frequencies that would foster high synchrony,[82,83] but has not previously been shown directly between neurons in prefrontal cortex and striatum. Overall, our results agree with those of the numerous studies examining cross-structural gamma coupling with 4 Hz and theta in this and related pathways,[26,28,34,84] with the gamma-80 oscillations serving as a more precisely synchronizing influence. Indeed, gamma oscillations have been

proposed to shape the formation of cell assemblies.[2,85] The one-quarter-cycle (~3 ms) difference of phase-locking of STR and PFC spikes to gamma-80 is consistent with the strong synchrony of the onset of gamma-80 bursts in PFC and vSTR LFPs, with PFC leading,[82] although the phase lag in the latter paper averaged only 0.59 ms. While the origin of many rhythms in STR and PFC remains unclear,[26,73,] their modulation of single neurons provides evidence that they are not simply volume-conduction artifacts here.

Behavioral correlates of distributed cell assemblies

The PFC-STR assemblies had behavioral correlates relevant for executing the present task requiring cognitive flexibility. Previous work has shown rule selectivity in STR and PFC.[39,86] In contrast with rule-selective responses, here assemblies, as well as individual STR and PFC neurons, had different activation rates in the same task (VD1 versus VD2), and these had a higher incidence than other comparisons. This is consistent with previous PFC population analyses revealing discrimination between repetitions of the same rule later in a behavioral session.[42,87] This has been only rarely reported in single neurons in STR.[88]

The observation of significant, task-relevant behavioral correlates in some assemblies where none of the members had that same correlate is consistent with properties emerging from integrative processes.[1,2] While it is possible that these correlates could have significance in other members of the assembly that we did not record, their absence in so many members highlights interesting properties of collective neural behavior.

To our knowledge, this is the first report of behavioral correlated activity of assemblies in a distributed neocortical-subcortical network. Previous studies of such correlates in single-structure assemblies could well represent only a part of more extensively distributed network activity. Indeed, when we observed assemblies limited to a single structure, this generally occurred when there was weaker sampling of the other structure. We propose that cross-structural assemblies are likely to be a general mechanism that extends to other brain areas and networks and underlie other highly integrated representations.

STAR★METHODS

Detailed methods are provided in the online version of this paper and include the following:

- KEY RESOURCES TABLE
- RESOURCE AVAILABILITY
  - Lead contact
  - Materials availability
  - Data and code availability
- EXPERIMENTAL MODEL AND SUBJECT DETAILS
- METHOD DETAILS
  - Pretraining
  - Surgery
  - Experimental design
  - The automated T-maze with return arms
  - Recordings
  - Histology and electrode position verification
  - Behavioral protocol
  - Sleep detection
- QUANTIFICATION AND STATISTICAL ANALYSIS
  - Cell assembly detection
  - Matching assemblies calculated with different bin widths
  - Asymmetry of the cross-correlations of STR-PFC cell pairs
  - Local field potential (LFP) analyses
  - Granger causality analysis
  - Spike-LFP analyses
  - Comparison of phase-locking in members and assemblies
  - Gamma burst detection
  - Cell activity analyses
  - Spatial distribution of neuron firing
  - Monte Carlo bootstrap analyses
  - Slope correction
  - Support Vector Machine analysis
  - Comparison of behavioral correlates of assemblies versus their members lacking significance for the correlate

SUPPLEMENTAL INFORMATION

Supplemental information can be found online at https://doi.org/10.1016/j.cub.2021.10.007.

ACKNOWLEDGMENTS

Support came from Agence Nationale de la Recherche ANR-2010-BLAN-0217-01 Neurobot, French Ministry of Research, MEMOLIFE Laboratory of Excellence, and Fondation Bettencourt Schueller. Thanks to France Maloumian for help preparing figures, Marie-Annick Thomas and Suzette Doutremer for training and advice for histology, Yves Dupraz for mechanical engineering, Nicole Quenech'du and Jérémie Teillon for advice and training for image processing, and Drs. M. Khamassi, C. Lansink, J. Matsumoto, and C. Lena for helpful suggestions.

AUTHOR CONTRIBUTIONS

S.I.W., V.J.O., and H.G. designed the study. V.J.O. and H.G. performed the experiments. V.J.O., C.J.B., R.T., S.I.W., and M.B.Z. designed the analyses. V.J.O. and C.J.B. performed the analyses. V.J.O., S.I.W., C.J.B., and M.B.Z. wrote the manuscript.

DECLARATION OF INTERESTS

The authors declare no competing interests.

Received: March 18, 2021
Revised: September 3, 2021
Accepted: October 4, 2021
Published: October 25, 2021

REFERENCES

1. Hebb, D.O. (1949). The Organization of Behavior (Wiley and Sons).
2. Buzsáki, G. (2010). Neural syntax: cell assemblies, synapsembles, and readers. Neuron *68*, 362–385.
3. Harris, K.D., Csicsvari, J., Hirase, H., Dragoi, G., and Buzsáki, G. (2003). Organization of cell assemblies in the hippocampus. Nature *424*, 552–556.
4. Uhlhaas, P.J., Pipa, G., Lima, B., Melloni, L., Neuenschwander, S., Nikolić, D., and Singer, W. (2009). Neural synchrony in cortical networks: history, concept and current status. Front. Integr. Nuerosci. *3*, 17.

5. Peyrache, A., Khamassi, M., Benchenane, K., Wiener, S.I., and Battaglia, F.P. (2009). Replay of rule-learning related neural patterns in the prefrontal cortex during sleep. Nat. Neurosci. *12*, 919–926.
6. Lansink, C.S., Goltstein, P.M., Lankelma, J.V., Joosten, R.N., McNaughton, B.L., and Pennartz, C.M. (2008). Preferential reactivation of motivationally relevant information in the ventral striatum. J. Neurosci. *28*, 6372–6382.
7. Sjulson, L., Peyrache, A., Cumpelik, A., Cassataro, D., and Buzsáki, G. (2018). Cocaine place conditioning strengthens location-specific hippocampal coupling to the nucleus accumbens. Neuron *98*, 926–934.e5.
8. Trouche, S., Koren, V., Doig, N.M., Ellender, T.J., El-Gaby, M., Lopes-Dos-Santos, V., Reeve, H.M., Perestenko, P.V., Garas, F.N., Magill, P.J., et al. (2019). A hippocampus-accumbens tripartite neuronal motif guides appetitive memory in space. Cell *176*, 1393–1406.e16.
9. Koch, C., Rapp, M., and Segev, I. (1996). A brief history of time (constants). Cereb. Cortex *6*, 93–101.
10. Markram, H., Lübke, J., Frotscher, M., and Sakmann, B. (1997). Regulation of synaptic efficacy by coincidence of postsynaptic APs and EPSPs. Science *275*, 213–215.
11. Magee, J.C., and Johnston, D. (1997). A synaptically controlled, associative signal for Hebbian plasticity in hippocampal neurons. Science *275*, 209–213.
12. Canolty, R.T., Ganguly, K., Kennerley, S.W., Cadieu, C.F., Koepsell, K., Wallis, J.D., and Carmena, J.M. (2010). Oscillatory phase coupling coordinates anatomically dispersed functional cell assemblies. Proc. Natl. Acad. Sci. USA *107*, 17356–17361.
13. Deolindo, C.S., Kunicki, A.C.B., da Silva, M.I., Lima Brasil, F., and Moioli, R.C. (2018). Neuronal assemblies evidence distributed interactions within a tactile discrimination task in rats. Front. Neural Circuits *11*, 114.
14. Mogenson, G.J., Jones, D.L., and Yim, C.Y. (1980). From motivation to action: functional interface between the limbic system and the motor system. Prog. Neurobiol. *14*, 69–97.
15. Haber, S.N. (2016). Corticostriatal circuitry. Dialogues Clin. Neurosci. *18*, 7–21.
16. Alexander, G.E., DeLong, M.R., and Strick, P.L. (1986). Parallel organization of functionally segregated circuits linking basal ganglia and cortex. Annu. Rev. Neurosci. *9*, 357–381.
17. Lansink, C.S., Goltstein, P.M., Lankelma, J.V., McNaughton, B.L., and Pennartz, C.M. (2009). Hippocampus leads ventral striatum in replay of place-reward information. PLoS Biol. *7*, e1000173.
18. Tingley, D., and Buzsáki, G. (2018). Transformation of a spatial map across the hippocampal-lateral septal circuit. Neuron *98*, 1229–1242.e5.
19. Peyrache, A., Lacroix, M.M., Petersen, P.C., and Buzsáki, G. (2015). Internally organized mechanisms of the head direction sense. Nat. Neurosci. *18*, 569–575.
20. Fries, P. (2015). Rhythms for cognition: communication through coherence. Neuron *88*, 220–235.
21. Pennartz, C.M., Berke, J.D., Graybiel, A.M., Ito, R., Lansink, C.S., van der Meer, M., Redish, A.D., Smith, K.S., and Voorn, P. (2009). Corticostriatal interactions during learning, memory processing, and decision making. J. Neurosci. *29*, 12831–12838.
22. Benchenane, K., Tiesinga, P.H., and Battaglia, F.P. (2011). Oscillations in the prefrontal cortex: a gateway to memory and attention. Curr. Opin. Neurobiol. *21*, 475–485.
23. van der Meer, M.A.A., Kalenscher, T., Lansink, C.S., Pennartz, C.M., Berke, J.D., and Redish, A.D. (2010). Integrating early results on ventral striatal gamma oscillations in the rat. Front. Neurosci. *4*, 300.
24. Berke, J.D., Breck, J.T., and Eichenbaum, H. (2009). Striatal versus hippocampal representations during win-stay maze performance. J. Neurophysiol. *101*, 1575–1587.
25. Berke, J.D., Okatan, M., Skurski, J., and Eichenbaum, H.B. (2004). Oscillatory entrainment of striatal neurons in freely moving rats. Neuron *43*, 883–896.
26. Tort, A.B., Kramer, M.A., Thorn, C., Gibson, D.J., Kubota, Y., Graybiel, A.M., and Kopell, N.J. (2008). Dynamic cross-frequency couplings of local field potential oscillations in rat striatum and hippocampus during performance of a T-maze task. Proc. Natl. Acad. Sci. USA *105*, 20517–20522.
27. Benchenane, K., Peyrache, A., Khamassi, M., Tierney, P.L., Gioanni, Y., Battaglia, F.P., and Wiener, S.I. (2010). Coherent theta oscillations and reorganization of spike timing in the hippocampal- prefrontal network upon learning. Neuron *66*, 921–936.
28. Fujisawa, S., and Buzsáki, G. (2011). A 4 Hz oscillation adaptively synchronizes prefrontal, VTA, and hippocampal activities. Neuron *72*, 153–165.
29. DeCoteau, W.E., Thorn, C., Gibson, D.J., Courtemanche, R., Mitra, P., Kubota, Y., and Graybiel, A.M. (2007). Learning-related coordination of striatal and hippocampal theta rhythms during acquisition of a procedural maze task. Proc. Natl. Acad. Sci. USA *104*, 5644–5649.
30. van der Meer, M.A.A., and Redish, A.D. (2011). Theta phase precession in rat ventral striatum links place and reward information. J. Neurosci. *31*, 2843–2854.
31. Weineck, K., García-Rosales, F., and Hechavarría, J.C. (2020). Neural oscillations in the fronto-striatal network predict vocal output in bats. PLoS Biol. *18*, e3000658.
32. Antzoulatos, E.G., and Miller, E.K. (2014). Increases in functional connectivity between prefrontal cortex and striatum during category learning. Neuron *83*, 216–225.
33. Koralek, A.C., Costa, R.M., and Carmena, J.M. (2013). Temporally precise cell-specific coherence develops in corticostriatal networks during learning. Neuron *79*, 865–872.
34. Donnelly, N.A., Holtzman, T., Rich, P.D., Nevado-Holgado, A.J., Fernando, A.B.P., Van Dijck, G., Holzhammer, T., Paul, O., Ruther, P., Paulsen, O., et al. (2014). Oscillatory activity in the medial prefrontal cortex and nucleus accumbens correlates with impulsivity and reward outcome. PLoS ONE *9*, e111300.
35. Ragozzino, M.E. (2007). The contribution of the medial prefrontal cortex, orbitofrontal cortex, and dorsomedial striatum to behavioral flexibility. Ann. N Y Acad. Sci. *1121*, 355–375.
36. Floresco, S.B., Ghods-Sharifi, S., Vexelman, C., and Magyar, O. (2006). Dissociable roles for the nucleus accumbens core and shell in regulating set shifting. J. Neurosci. *26*, 2449–2457.
37. Oualian, C., and Gisquet-Verrier, P. (2010). The differential involvement of the prelimbic and infralimbic cortices in response conflict affects behavioral flexibility in rats trained in a new automated strategy-switching task. Learn. Mem. *17*, 654–668.
38. Hart, G., Leung, B.K., and Balleine, B.W. (2014). Dorsal and ventral streams: the distinct role of striatal subregions in the acquisition and performance of goal-directed actions. Neurobiol. Learn. Mem. *108*, 104–118.
39. Bissonette, G.B., and Roesch, M.R. (2015). Rule encoding in dorsal striatum impacts action selection. Eur. J. Neurosci. *42*, 2555–2567.
40. Fino, E., and Venance, L. (2011). Spike-timing dependent plasticity in striatal interneurons. Neuropharmacology *60*, 780–788.
41. Friedman, A., Homma, D., Gibb, L.G., Amemori, K., Rubin, S.J., Hood, A.S., Riad, M.H., and Graybiel, A.M. (2015). A corticostriatal path targeting striosomes controls decision-making under conflict. Cell *161*, 1320–1333.
42. Malagon-Vina, H., Ciocchi, S., Passecker, J., Dorffner, G., and Klausberger, T. (2018). Fluid network dynamics in the prefrontal cortex during multiple strategy switching. Nat. Commun. *9*, 309.
43. Maingret, N., Girardeau, G., Todorova, R., Goutierre, M., and Zugaro, M. (2016). Hippocampo-cortical coupling mediates memory consolidation during sleep. Nat. Neurosci. *19*, 959–964.
44. Todorova, R., and Zugaro, M. (2019). Isolated cortical computations during delta waves support memory consolidation. Science *366*, 377–381.

45. Sakurai, Y., Nakazono, T., Ishino, S., Terada, S., Yamaguchi, K., and Takahashi, S. (2013). Diverse synchrony of firing reflects diverse cell-assembly coding in the prefrontal cortex. J. Physiol. Paris *107*, 459–470.

46. Lansink, C.S., Goltstein, P.M., Lankelma, J.V., and Pennartz, C.M. (2010). Fast-spiking interneurons of the rat ventral striatum: temporal coordination of activity with principal cells and responsiveness to reward. Eur. J. Neurosci. *32*, 494–508.

47. Bakhurin, K.I., Mac, V., Golshani, P., and Masmanidis, S.C. (2016). Temporal correlations among functionally specialized striatal neural ensembles in reward-conditioned mice. J. Neurophysiol. *115*, 1521–1532.

48. Pennartz, C.M., Lee, E., Verheul, J., Lipa, P., Barnes, C.A., and McNaughton, B.L. (2004). The ventral striatum in off-line processing: ensemble reactivation during sleep and modulation by hippocampal ripples. J. Neurosci. *24*, 6446–6456.

49. Dejean, C., Courtin, J., Karalis, N., Chaudun, F., Wurtz, H., Bienvenu, T.C., and Herry, C. (2016). Prefrontal neuronal assemblies temporally control fear behaviour. Nature *535*, 420–424.

50. Roy, S.A., and Alloway, K.D. (2001). Coincidence detection or temporal integration? What the neurons in somatosensory cortex are doing. J. Neurosci. *21*, 2462–2473.

51. Ito, M., and Doya, K. (2015). Distinct neural representation in the dorsolateral, dorsomedial, and ventral parts of the striatum during fixed- and free-choice tasks. J. Neurosci. *35*, 3499–3514.

52. Seamans, J.K., Floresco, S.B., and Phillips, A.G. (1995). Functional differences between the prelimbic and anterior cingulate regions of the rat prefrontal cortex. Behav. Neurosci. *109*, 1063–1073.

53. Sierra-Mercado, D., Padilla-Coreano, N., and Quirk, G.J. (2011). Dissociable roles of prelimbic and infralimbic cortices, ventral hippocampus, and basolateral amygdala in the expression and extinction of conditioned fear. Neuropsychopharmacology *36*, 529–538.

54. Mailly, P., Aliane, V., Groenewegen, H.J., Haber, S.N., and Deniau, J.-M. (2013). The rat prefrontostriatal system analyzed in 3D: evidence for multiple interacting functional units. J. Neurosci. *33*, 5718–5727.

55. Geisler, C., Robbe, D., Zugaro, M., Sirota, A., and Buzsáki, G. (2007). Hippocampal place cell assemblies are speed-controlled oscillators. Proc. Natl. Acad. Sci. USA *104*, 8149–8154.

56. Mallet, N., Le Moine, C., Charpier, S., and Gonon, F. (2005). Feedforward inhibition of projection neurons by fast-spiking GABA interneurons in the rat striatum in vivo. J. Neurosci. *25*, 3857–3869.

57. Koos, T., Tepper, J.M., and Wilson, C.J. (2004). Comparison of IPSCs evoked by spiny and fast-spiking neurons in the neostriatum. J. Neurosci. *24*, 7916–7922.

58. Humphries, M.D., Wood, R., and Gurney, K. (2009). Dopamine-modulated dynamic cell assemblies generated by the GABAergic striatal microcircuit. Neural Netw. *22*, 1174–1188.

59. Ponzi, A., and Wickens, J. (2012). Input dependent cell assembly dynamics in a model of the striatal medium spiny neuron network. Front. Syst. Neurosci. *6*, 6.

60. Butler, W.N., and Taube, J.S. (2017). Oscillatory synchrony between head direction cells recorded bilaterally in the anterodorsal thalamic nuclei. J. Neurophysiol. *117*, 1847–1852.

61. Sala-Bayo, J., Fiddian, L., Nilsson, S.R.O., Hervig, M.E., McKenzie, C., Mareschi, A., Boulos, M., Zhukovsky, P., Nicholson, J., Dalley, J.W., et al. (2020). Dorsal and ventral striatal dopamine D1 and D2 receptors differentially modulate distinct phases of serial visual reversal learning. Neuropsychopharmacology *45*, 736–744.

62. Gireesh, E.D., and Plenz, D. (2008). Neuronal avalanches organize as nested theta- and beta/gamma-oscillations during development of cortical layer 2/3. Proc. Natl. Acad. Sci. USA *105*, 7576–7581.

63. Thorn, C.A., and Graybiel, A.M. (2014). Differential entrainment and learning-related dynamics of spike and local field potential activity in the sensorimotor and associative striatum. J. Neurosci. *34*, 2845–2859.

64. Pouzzner, D. (2020). Control of functional connectivity in cerebral cortex by basal ganglia mediated synchronization. arXiv, arXiv:1708.00779v2. https://arxiv.org/abs/1708.00779.

65. Williams, D., Tijssen, M., Van Bruggen, G., Bosch, A., Insola, A., Di Lazzaro, V., Mazzone, P., Oliviero, A., Quartarone, A., Speelman, H., and Brown, P. (2002). Dopamine-dependent changes in the functional connectivity between basal ganglia and cerebral cortex in humans. Brain *125*, 1558–1569.

66. Cardoso-Cruz, H., Sousa, M., Vieira, J.B., Lima, D., and Galhardo, V. (2013). Prefrontal cortex and mediodorsal thalamus reduced connectivity is associated with spatial working memory impairment in rats with inflammatory pain. Pain *154*, 2397–2406.

67. Cohen, M.X., Bour, L., Mantione, M., Figee, M., Vink, M., Tijssen, M.A., van Rootselaar, A.F., van den Munckhof, P., Schuurman, P.R., and Denys, D. (2012). Top-down-directed synchrony from medial frontal cortex to nucleus accumbens during reward anticipation. Hum. Brain Mapp. *33*, 246–252.

68. Kelley, R., Flouty, O., Emmons, E.B., Kim, Y., Kingyon, J., Wessel, J.R., Oya, H., Greenlee, J.D., and Narayanan, N.S. (2018). A human prefrontal-subthalamic circuit for cognitive control. Brain *141*, 205–216.

69. Rodriguez, E., George, N., Lachaux, J.P., Martinerie, J., Renault, B., and Varela, F.J. (1999). Perception's shadow: long-distance synchronization of human brain activity. Nature *397*, 430–433.

70. Arnulfo, G., Wang, S.H., Myrov, V., Toselli, B., Hirvonen, J., Fato, M.M., Nobili, L., Cardinale, F., Rubino, A., Zhigalov, A., et al. (2020). Long-range phase synchronization of high-frequency oscillations in human cortex. Nat. Commun. *11*, 5363.

71. Huang, Y., Yaple, Z.A., and Yu, R. (2020). Goal-oriented and habitual decisions: neural signatures of model-based and model-free learning. Neuroimage *215*, 116834.

72. Karalis, N., Dejean, C., Chaudun, F., Khoder, S., Rozeske, R.R., Wurtz, H., Bagur, S., Benchenane, K., Sirota, A., Courtin, J., and Herry, C. (2016). 4-Hz oscillations synchronize prefrontal-amygdala circuits during fear behavior. Nat. Neurosci. *19*, 605–612.

73. Carmichael, J.E., Gmaz, J.M., and van der Meer, M.A.A. (2017). Gamma oscillations in the rat ventral striatum originate in the piriform cortex. J. Neurosci. *37*, 7962–7974.

74. Tort, A.B.L., Ponsel, S., Jessberger, J., Yanovsky, Y., Brankačk, J., and Draguhn, A. (2018). Parallel detection of theta and respiration-coupled oscillations throughout the mouse brain. Sci. Rep. *8*, 6432.

75. Tabuchi, E.T., Mulder, A.B., and Wiener, S.I. (2000). Position and behavioral modulation of synchronization of hippocampal and accumbens neuronal discharges in freely moving rats. Hippocampus *10*, 717–728.

76. Jones, M.W., and Wilson, M.A. (2005). Phase precession of medial prefrontal cortical activity relative to the hippocampal theta rhythm. Hippocampus *15*, 867–873.

77. Gruber, A.J., Hussain, R.J., and O'Donnell, P. (2009). The nucleus accumbens: a switchboard for goal-directed behaviors. PLoS ONE *4*, e5062.

78. Stenner, M.-P., Litvak, V., Rutledge, R.B., Zaehle, T., Schmitt, F.C., Voges, J., Heinze, H.-J., and Dolan, R.J. (2015). Cortical drive of low-frequency oscillations in the human nucleus accumbens during action selection. J. Neurophysiol. *114*, 29–39.

79. Horschig, J.M., Smolders, R., Bonnefond, M., Schoffelen, J.-M., van den Munckhof, P., Schuurman, P.R., Cools, R., Denys, D., and Jensen, O. (2015). Directed communication between nucleus accumbens and neocortex in humans is differentially supported by synchronization in the theta and alpha band. PLoS ONE *10*, e0138685.

80. Costa, R.M., Lin, S.C., Sotnikova, T.D., Cyr, M., Gainetdinov, R.R., Caron, M.G., and Nicolelis, M.A. (2006). Rapid alterations in corticostriatal ensemble coordination during acute dopamine-dependent motor dysfunction. Neuron *52*, 359–369.

81. Akam, T., and Kullmann, D.M. (2014). Oscillatory multiplexing of population codes for selective communication in the mammalian brain. Nat. Rev. Neurosci. *15*, 111–122.

82. Catanese, J., Carmichael, J.E., and van der Meer, M.A.A. (2016). Low- and high-gamma oscillations deviate in opposite directions from zero-phase synchrony in the limbic corticostriatal loop. J. Neurophysiol. *116*, 5–17.

83. von Nicolai, C., Engler, G., Sharott, A., Engel, A.K., Moll, C.K., and Siegel, M. (2014). Corticostriatal coordination through coherent phase-amplitude coupling. J. Neurosci. *34*, 5938–5948.

84. Igarashi, J., Isomura, Y., Arai, K., Harukuni, R., and Fukai, T. (2013). A θ-γ oscillation code for neuronal coordination during motor behavior. J. Neurosci. *33*, 18515–18530.

85. Engel, A.K., Fries, P., and Singer, W. (2001). Dynamic predictions: oscillations and synchrony in top-down processing. Nat. Rev. Neurosci. *2*, 704–716.

86. Asaad, W.F., Rainer, G., and Miller, E.K. (1998). Neural activity in the primate prefrontal cortex during associative learning. Neuron *21*, 1399–1407.

87. Guise, K.G., and Shapiro, M.L. (2017). Medial prefrontal cortex reduces memory interference by modifying hippocampal encoding. Neuron *94*, 183–192.e8.

88. Shibata, R., Mulder, A.B., Trullier, O., and Wiener, S.I. (2001). Position sensitivity in phasically discharging nucleus accumbens neurons of rats alternating between tasks requiring complementary types of spatial cues. Neuroscience *108*, 391–411.

89. Wood, E.R., Dudchenko, P.A., Robitsek, R.J., and Eichenbaum, H. (2000). Hippocampal neurons encode information about different types of memory episodes occurring in the same location. Neuron *27*, 623–633.

90. Catanese, J., Cerasti, E., Zugaro, M., Viggiano, A., and Wiener, S.I. (2012). Dynamics of decision-related activity in hippocampus. Hippocampus *22*, 1901–1911.

91. Hazan, L., Zugaro, M., and Buzsáki, G. (2006). Klusters, NeuroScope, NDManager: a free software suite for neurophysiological data processing and visualization. J. Neurosci. Methods *155*, 207–216.

92. Marčenko, V.A., and Pastur, L.A. (1967). Distribution of eigenvalues in certain sets of random matrices. Math. USSR-Sbornik *1*, 457–483.

93. Lopes-dos-Santos, V., Ribeiro, S., and Tort, A.B. (2013). Detecting cell assemblies in large neuronal populations. J. Neurosci. Methods *220*, 149–166.

94. Russo, E., and Durstewitz, D. (2017). Cell assemblies at multiple time scales with arbitrary lag constellations. eLife *6*, e19428.

95. Pfeiffer, B.E., and Foster, D.J. (2015). PLACE CELLS. Autoassociative dynamics in the generation of sequences of hippocampal place cells. Science *349*, 180–183.

96. Belluscio, M.A., Mizuseki, K., Schmidt, R., Kempter, R., and Buzsáki, G. (2012). Cross-frequency phase-phase coupling between θ and γ oscillations in the hippocampus. J. Neurosci. *32*, 423–435.

97. Lalla, L., Rueda Orozco, P.E., Jurado-Parras, M.-T., Brovelli, A., and Robbe, D. (2017). Local or not local: Investigating the nature of striatal theta oscillations in behaving rats. eNeuro *4*, ENEURO.0128-17.2017.

98. Oostenveld, R., Fries, P., Maris, E., and Schoffelen, J.M. (2011). FieldTrip: open source software for advanced analysis of MEG, EEG, and invasive electrophysiological data. Comput. Intell. Neurosci. *2011*, 156869.

99. Dhamala, M., Rangarajan, G., and Ding, M. (2008). Estimating Granger causality from fourier and wavelet transforms of time series data. Phys. Rev. Lett. *100*, 018701.

100. Vinck, M., Battaglia, F.P., Womelsdorf, T., and Pennartz, C. (2012). Improved measures of phase-coupling between spikes and the local field potential. J. Comput. Neurosci. *33*, 53–75.

101. López-Madrona, V.J., Pérez-Montoyo, E., Álvarez-Salvado, E., Moratal, D., Herreras, O., Pereda, E., Mirasso, C.R., and Canals, S. (2020). Different theta frameworks coexist in the rat hippocampus and are coordinated during memory-guided and novelty tasks. eLife *9*, e57313.

102. Fujisawa, S., Amarasingham, A., Harrison, M.T., and Buzsáki, G. (2008). Behavior-dependent short-term assembly dynamics in the medial prefrontal cortex. Nat. Neurosci. *11*, 823–833.

103. Siapas, A.G., Lubenov, E.V., and Wilson, M.A. (2005). Prefrontal phase locking to hippocampal theta oscillations. Neuron *46*, 141–151.

104. Barthó, P., Hirase, H., Monconduit, L., Zugaro, M., Harris, K.D., and Buzsáki, G. (2004). Characterization of neocortical principal cells and interneurons by network interactions and extracellular features. J. Neurophysiol. *92*, 600–608.

STAR★METHODS

KEY RESOURCES TABLE

REAGENT or RESOURCE	SOURCE	IDENTIFIER
Chemicals, peptides, and recombinant proteins		
Xylazine (Rompun 2%)	Bayer	N/A
Sodium pentobarbital (Euthasol)	DECHRA	N/A
Deposited data		
Raw data	CRCNS.org	https://doi.org/10.6080/K0R20ZKP
Experimental models: Organisms/strains		
Long-Evans male adult rats	René Janvier, Genest-St-Isle, France	RRID: RGD_2308852
Software and algorithms		
FMAToolbox (statistical toolbox)	http://fmatoolbox.sourceforge.net).	RRID: SCR_015533
MATLAB Chronux toolbox	http://www.chronux.org	RRID: SCR_005547
fastICA algorithm for MATLAB	http://research.ics.aalto.fi/ica/fastica	RRID: SCR_013110
KlustaKwik	http://klustakwik.sourceforge.net	RRID: SCR_014480
Klusters	http://neurosuite.sourceforge.net	RRID: SCR_008020
Fieldtrip toolbox (Oostenveld et al., 2011)	http://www.fieldtriptoolbox.org	RRID: SCR_004849
support vector machines (SVMs) from the libSVM library	https://www.csie.ntu.edu.tw/∼cjlin/libsvm	RRID: SCR_010243

RESOURCE AVAILABILITY

Lead contact

Further information and requests for resources should be directed to and will be fulfilled by the lead contact, Sidney Wiener (sidney.wiener@college-de-france.fr).

Materials availability

This study did not generate new unique reagents. Instructions for constructing the custom microdrive will be furnished upon request.

Data and code availability

All data needed to evaluate the conclusions in the paper are present in the paper, the supplemental information, and at https://doi.org/10.6080/K0R20ZKP.

EXPERIMENTAL MODEL AND SUBJECT DETAILS

Six adult (weight 350–400 g) male Long-Evans rats (RRID: RGD_2308852) were housed on a 12:12-h light-dark cycle. Experiments were performed during the day in facilities authorized by the Veterinary Services of the city of Paris (n° B75-05-12). Rats were handled each workday in the experimental room. Rats were housed individually to permit control of partial water deprivation (below).

METHOD DETAILS

Pretraining

Rats were first familiarized with the experimental environment by free exploration of the maze (foraging for scattered pieces of chocolate puffed rice breakfast cereal) for at least three days. When the pre-training and training began, animals were partially water-restricted (10 min per day or more as required) to no less than 85% of their free-feeding weight. All procedures were in accord with local (autorisation d'expérimenter n°75-1328-R; Comité d'Ethique pour l'Expérimentation Animale no. 59, dossier 2012-0007) and international (European Directive 2010/63/EU; US National Institutes of Health guidelines) standards and legal regulations regarding the use and care of animals.

Surgery

Rats were allowed at least 2 days before surgery with *ad libitum* water and no training. Rats were deeply anesthetized (xylazine, 20 mg/ml, 0.1 mL intramuscular; sodium pentobarbital, 40 mg per kg of body weight, intraperitoneal, with a 5 mg supplement i.p. every hour as needed). The head was placed in a Kopf stereotaxic instrument, the cranial surface was prepared, jeweler's screws were attached with dental cement reinforcement, and trephination was performed. Then rats were implanted with a custom-built microdrive

holding 15 independently movable tetrodes (groups of four twisted 13 μm tungsten wires, gold-plated to ~200 kOhm). Usually eight tetrodes were placed in the ventral or dorso-medial STR (AP 1.0-2.5 mm and ML 0.8–1.8 mm relative to bregma), and seven in the medial prefrontal cortex (AP 2.5–3.4 mm and ML 0.3–0.9 mm). The implant was secured to the skull screws with dental cement. Miniature stainless steel screws were implanted above the cerebellum as reference and ground electrodes. After surgery, rats were allowed to recover for at least one week with *ad libitum* food and water, before any further training. The electrodes were then progressively lowered until they reached their targets and then adjusted every day to optimize unit isolation and recording quality.

Experimental design

Neuronal activity was recorded as the rats performed in a completely automated maze, or during sleep immediately preceding and following this. Relevant analyses compared activity between series of criterion performance trials when the rats were exposed to the same cues and performed the same movements, but with different rules. Each neuron served as its own control and activity levels were compared before versus after events with analyses and statistical tests as described in the following sections. Since the neuronal activity is not necessarily normally distributed and is dependent on behavior, Monte Carlo bootstrap analyses were employed (detailed below) since they examine the distribution of each cell's activity individually without making assumptions of normality. The number of replicates and sample size (see Tables S1–S3) were chosen to be sufficient to provide reasonably low variances and statistically credible results.

The automated T-maze with return arms

(See Figure 4A; *cf.* Wood et al.[89] and Catanese et al.[90]). The experimental chamber was a 3 m diameter cylindrical space, enclosed by black curtains running from floor to ceiling and was lit by a ceiling mounted light bulb. The maze was constructed from matte black painted wood. Maze arms were 8 cm wide with 2 cm high borders. The central arm was 1 m long and the reward arms were each 50 cm long. At the junction of the return arms and the central arm was a return/start zone measuring 35x38 cm. The maze was elevated 70 cm above the floor. The experimental protocol was automated and paced by the rat. As the rat spontaneously crossed a photodetector near the beginning of the central arm ('C' in Figure 4A), this triggered the display of visual cues on two TV screens (80 cm diagonal; 76 cm above the floor) centered behind the two reward sites. The visual cues were vertical bars (spatial frequency of 0.13 cycles per degree) projected on one screen and horizontal bars on the other, or, in later experiments, to facilitate learning, simply one white and one black screen. Following correct choices, a photodetector on the reward arm ('W') triggered distribution of a saccharinated (0.25%, 30 μl) water reward via a solenoid valve controlled by a CED Power1401 interface (Cambridge, UK) with our scripts. Cues remained on until the rat crossed the photodetector at the middle of the return arm ('P').

Recordings

Brain signals were pre-amplified (unity-gain headstage, Noted Bt, Pécs, Hungary), amplified 500x (Neuralynx L8, Neuralynx, Bozeman, MT, USA), acquired and digitized with two synchronized CED Power1401 interfaces. To track the position of the animal, two light–emitting diodes were fixed to the front of the head-mounted microdrive. These were detected by an overhead video camera (sampling rate 30 Hz).

Histology and electrode position verification

To confirm recording sites, electrolytic lesions (cathodal current injection: 30 μA for 30 s) were applied to each tetrode. Two days later, the rats were administered a lethal dose of pentobarbital and were intracardially perfused with saline (0.9%, wt/vol) followed by paraformaldehyde solution (10%, wt/vol). Brain regions of interest were sliced into 40 μm coronal sections and stained with cresyl violet. For 3 of the rats, prior to implant surgery, electrode tips were dipped in fluorescent marking dyes (Sigma-Aldrich). In those cases, half of the histology sections were set aside for fluorescence microscopy observations. Electrode positions were then reconstructed in 3D with the Neurolucida system (MBF Bioscience, Williston, VT 05495 USA, https://www.mbfbioscience.com/neurolucida) on the basis of lesion location and the depths the electrodes had been lowered. Only data from electrodes with confirmed recording locations were further analyzed.

Behavioral protocol

During the pre-training phase (10 ± 3 days, mean ± SD), the rats were trained to follow forward paths on the T-maze. Backtracking was prevented with manual placement of transparent Plexiglas barriers or a pulley-driven barrier on the reward arms. Rats were trained on the T-maze to acquire and alternate between the two tasks. Daily training and recording sessions consisted of one or two blocks of 20-30 min (the average time to perform one trial was 25 ± 1.5 s). On average, post-surgery training and recording sessions for a given rat lasted about 90 days. In order to obtain liquid rewards, the rats had to visit the correct arm according to the current rule. Visual cues were displayed on the two screens in pseudorandom order: each screen did not display the same cue more than four times successively. First, in the visual cue task (VD), one cue indicated the rewarded arm, irrespective of whether it was to the left or right (Figure 4B). Once the rat reached a criterion of a minimum of 10 consecutive correct trials, or 80% correct choices for the whole session, in the following session training commenced in the spatial discrimination task (SD). In the SD task, reward was provided on only one (right or left) arm, irrespective of the visual cue displays. This was selected as their non-preferred arm, as determined during pre-training. Once the rat reached the same criterion performance as above, the next session started with retraining in a few more VD sessions.

Rats were then trained to flexibly switch between the two rules within the same session. Since the rats had found the VD task more difficult (27 ± 5 sessions for VD versus 2.0 ± 0.7 sessions for SD), the rule sequence of all sessions required the rats to first reach criterion (eight consecutive correct trials) in VD (these high performance trials are called "VD1"). Then the rule was changed to SD and the trials where the rat subsequently performed at criterion level are called "SD". Similarly, following the rule change back to VD (with the same cue contingency), the next series of criterion performance trials is referred to as "VD2". Data from the 20 sessions with criterion level performance in these three task conditions are presented here. There were no significant differences in overall performance between the first and last sessions (Wilcoxon signed-rank, n = 6 rats, p = 0.0625).

No cue (other than absence of reward) was presented for incorrect trials, and thus the rats learned by trial and error. The current rule was signaled by the presence (SD task) or absence (VD task) of a sound cue (repetition of the Microsoft Windows standard system 'Asterisk' sound) by a loudspeaker in front of the T-maze. The tone went on when the central arm photodetector was crossed and was turned off when the return arm photodetector was crossed. Rule changes were extra-dimensional, that is, between VD and SD. This protocol was designed so that the sensory inputs and motor outputs remained virtually the same in both tasks, permitting distinction of neural activity specific to the cognitive demands of the respective tasks.

Sleep detection

Each behavioral recording was preceded and followed by a rest/sleep recording session in a terra cotta flowerpot lined with a towel. These sessions lasted at least 10 min (2 of the 6 rats) or 1 hour (the other 4 rats). Sleep data were recorded in 10 of the sessions, when 58 of the assemblies were recorded.

Sleep was detected by low movement speed. Headstage LED signals were first smoothed and periods when the speed did not exceed 0.05 m/s for a duration of at least 120 s (with a tolerance of 2 s when this velocity could be exceeded).

QUANTIFICATION AND STATISTICAL ANALYSIS

Statistics are reported as the median ± 25% confidence intervals. Tests included the Kuiper's test, pairwise phase consistency (PPC), Spearman correlation, the Rayleigh statistic, the Kruskal-Wallis test (or, for paired data, the Friedman test), for post hoc tests, the Wilcoxon rank sum (or signed rank) test, with Bonferroni-corrected when necessary, and for proportion comparisons, the binomial test. The specific applications of these tests are explained in the Results section.

Offline spike sorting was carried out with Principal Component Analysis (PCA) with NDManager for preprocessing[91] (http://neurosuite.sourceforge.net), and a semi-automatic cluster cutting procedure combining KlustaKwik (K.D. Harris, http://klustakwik.sourceforge.net) and Klusters (L. Hazan, http://neurosuite.sourceforge.net).

Cell assembly detection

A method based on principal and independent component analyses (PCA and ICA) detected the co-activation of simultaneously recorded neurons referred to as "assemblies". First PCA was performed. The activity of the neurons during task performance sessions was binned into 30 ms time bins to build a spike matrix S, where S_{ij} represents the firing of neuron *i* in temporal bin *j*. The matrix was z-scored, resulting in the Z matrix, where the i-th row of Z represents the z-scored activity of neuron *i* over all temporal bins. We calculated Q, the pairwise cell activity correlation matrix where N is the total number of neurons. We then computed the eigenvalue decomposition of Q. Eigenvalues that exceeded the upper bounds of the Marčenko-Pastur distribution[92] were considered significant. However PCs are, by definition, orthogonal, a constraint that is not necessarily respected in the brain. To address this issue we carried out ICA on the major PCs[93] using the fast independent component analysis (fastICA) algorithm for MATLAB. This ICA returned assemblies as vectors of N weights, corresponding to the respective cell's contributions. Since the signs of the output weights are arbitrary, weights were inverted as necessary to render the highest absolute weight positive. Components were normalized such that a component with equal contribution from all N neurons recorded in a session would be composed of N equal weights each with absolute value $1/\sqrt{N}$. Thus, neurons with weights exceeding $1/\sqrt{N}$ are referred to as "assembly members". The activation strength of each assembly within a given time bin is computed by projecting the matrix Z (constructed with 30 ms bins and a 10 ms sliding window) onto a template matrix obtained by the matrix product of the component and its transpose. The diagonal of the template matrix is set to zero so that single neuron spiking does not contribute to the activation strength. Thus the activation strength is high when multiple neurons with high weights fire synchronously and increases when synchronous high weight neurons fire more. Assemblies were considered to be active when their activation strength exceeded 5, which corresponds to the median of the 99th quantile distribution of activation strength.

Note that the Marčenko-Pastur threshold is derived from a random matrices theorem and its use for selecting major principal components has been criticized.[94] To address this issue, we shuffled spike identity while preserving spike time stamps to create surrogate data and then ran PCA. This procedure was repeated 1000 times to build a distribution of eigenvalues. The 95% quantile of this distribution was considered as an alternative threshold to Marčenko-Pastur. No significant differences were found when comparing data from the Marčenko-Pastur threshold to the present one derived from surrogate data (p = 0.77; Wilcoxon paired rank test).

To control for whether the detected assemblies may have appeared by chance, we simulated a Poisson spike train dataset, where, in each bin, each neuron's spikes were replaced by generating Poisson-distributed numbers of spikes for each cell, according to its firing rate.[95] Since cell synchrony could appear by chance due to similar phase preferences to rhythmic activity or to similar spatial/behavioral correlates, the replacements were made taken into account the respective firing rates at four phases of 4 Hz or theta

rhythms (0 to pi/2, etc.), and in four different segments of the maze. Thus the simulated Poisson spike train is generated for these combinations of four zones and four phase ranges independently, then the simulated activity is merged, and the PCA-ICA is performed anew (this procedure was repeated 500 times for each session). This yielded averages of 0.31 ± 0.10 and 0.38 ± 0.10 assemblies per session for 4 Hz and theta respectively. When supplementary behavioral correlates (rewarded/unrewarded trials and right/left trials) were also taken into account this yielded only 0.50 ± 0.10 assemblies per session. (Note that sampling issues prevented segregation into more bins.) These were all much lower than the actual data (4.6 ± 0.5 assemblies per session; Kruskal-Wallis test, p = 2.54e-12 for n = 16 sessions). However, since a minor number of assemblies did appear with this control, we examined their robustness, as indicated by their eigenvalues. As expected, eigenvalues were considerably lower for the Poisson shuffled spike trains (1.16 versus 1.06, p = 8.33e-18, Wilcoxon signed rank test). Thus, this indicates that the assemblies detected here did not arise coincidentally due to similar behavioral correlates and/or common phase-locking.

Matching assemblies calculated with different bin widths

The PCA-ICA analyses of the dataset were performed with bin widths ranging from 10 to 150 ms. Assemblies detected at different timescales were iteratively matched by selecting pairs with maximum correlations (Spearman coefficient). First, we computed correlations between each possible pair of assemblies computed with two different bin widths. The pair with the highest coefficient was set aside and the procedure was repeated with the remaining assemblies until all assemblies were paired. When the number of assemblies was different from one timescale to another, the remaining assemblies were left unmatched. Matched pairs with significant Spearman coefficients were considered as ''highly correlated.''

Asymmetry of the cross-correlations of STR-PFC cell pairs

We calculated an asymmetry index (inspired by Belluscio et al.[96]): for each STR-PFC member pair, the normalized ratio of area under the positive part of the cross-correlogram curve (]0 ms, 30 ms]) over the area under the negative part ([-15 ms, 0 ms[). Thus when the index is positive, there are more cross-correlated STR spikes after the PFC spike, while when the ratio is negative, it is the opposite. A Wilcoxon sign rank test determined whether the median of the distribution was greater than zero.

Local field potential (LFP) analyses

LFPs were derived from wideband signals that had been down-sampled to 1250 Hz on all channels. Power spectra were calculated with wavelet methods. The spectrogram was also calculated with multi-taper Fourier methods. Since the results were similar for the two methods, the wavelet method was retained. These were performed for the entire session, and then averaged for each spatial bin. Spectra were normalized to 1/f. Since there is controversy about the origin of some STR LFP oscillations,[73,97] two types of signals were analyzed. ''Raw'' signals from a single STR tetrode wire were referenced to the cerebellar skull screw. To control for possible volume conduction and reference channel activity in STR, ''locally referenced signals'' were derived from a single STR tetrode wire, subtracting the average LFP recorded across the other tetrodes there for 4 and 8 Hz analyses. However, no major difference was observed compared to raw signals, so the latter are reported. Results were similar with only one selected channel by area or with the average of all recorded channels, only the former were used. Coherence calculations were based on a multi-taper Fourier analysis and performed with custom-written, MATLAB-based programs. We used the Chronux toolbox cohgramc() function with a time window of 2 s, a step size of 0.1 s and a bandwidth product of 3 with 5 tapers.

Granger causality analysis

To determine whether PFC oscillations precede STR oscillations, Granger causality was measured with the Fieldtrip toolbox.[98] We used non-parametric Granger causality based on Fourier transforms[99] within windows of 1 s for frequencies from 1 to 20 Hz.

Spike-LFP analyses

Since STR and PFC oscillation profiles were quite similar and the nature of STR oscillations is controversial, all analysis presented refer to PFC LFPs. To examine modulation of spiking activity by LFP oscillations, first instantaneous signal power and phase were derived from the Hilbert transform of the bandpass-filtered signal. We quantified phase consistency of spikes relative to the LFP band with both the Rayleigh test of circular uniformity and the unbiased pairwise phase consistency (PPC[100]). For each unit and assembly, we first tested for significant entrainment to the LFP at low frequencies: 4 Hz (from 2 to 6 Hz) and theta (from 6 to 12 Hz). Unlike humans, theta in behaving rats is in this range, typically peaking at 8 Hz,[101] while the range for 4 Hz was selected on the basis of the peak in the data (Figures 2A and 2B; also *cf.* Fujisawa et al.[102]). To characterize phase-locking in neurons, we used two methods. With the Rayleigh test, a neuron or an assembly was considered as phase-locked if $p < 0.05$ and kappa > 0.1. This criterion was chosen on the basis of k-means separation and confirmed by eye. Moreover, to take into account the non-uniformity of the signal (cycle asymmetry) we use the correction of Siapas et al.[103] Even though the main results did not change, we report the corrected data. In the second method (used for neurons only), PPC threshold was determined from a jitter analysis: in data from each single unit, spikes were randomly jittered within a time window equivalent to a single cycle of the band under study. The actual values were considered significant if they exceeded the 95th percentile of this distribution. Since the results were similar between the two methods, the Rayleigh result is reported.

Comparison of phase-locking in members and assemblies

To determine whether STR and PFC members were phase-locked only during assembly activations, modulation was compared between cycles containing assembly activations (“IN”) and other cycles (“OUT”). First instantaneous signal power and unwrap phase were derived from the Hilbert transform of the bandpass-filtered signal. Each individual cycle (multiples of 2*pi) was determined. For each assembly, if the cycle contained an activation, then it was IN, otherwise it was OUT. Then phase-locking was calculated individually for each member for IN and OUT, as described above. However since there was slight variability in the preferred phases among different assemblies, the difference between the assembly’s preferred phases and the actual spike phases were calculated for each member of each assembly (and were calculated separately for IN and OUT. Then the Kuiper test compared the IN and OUT circular distributions. Note that power was not significantly different in IN versus OUT cycles (Friedman test: $p > 0.05$) for both 4 and 8 Hz. Down-sampling the number of data points to balance them between IN and OUT yielded the same results

Gamma burst detection

We detected transient gamma burst events in both the STR and PFC LFPs. LFPs were first filtered in the high-gamma band (70–110 Hz) using the MATLAB *filtfilt* function (4th order Chebyshev filter). Instantaneous signal amplitude was obtained by taking the modulus of the Hilbert-transformed signal. Gamma events were defined as when the amplitude envelope exceeded the 95th percentile of the amplitude distribution and contained at least three gamma cycles. Events separated by less than 1/2 cycle were merged.

Cell activity analyses

A k-means analysis distinguished putative PFC and STR interneurons and principal cells based on spike waveform half-amplitude duration and trough-to-peak delay.[104] For STR neurons, a firing rate criterion was also applied.[25] The STR units were classified as putative MSN projection neurons (83%) or fast spiking interneurons (15%), leaving 2% unclassified. In the PFC recordings, these two waveform parameters alone permitted classification of 85% as projection neurons and 13% as interneurons, leaving 2% unclassified. Further analyses focused on neurons with average firing rates equal to or greater than 0.1 Hz.

Spatial distribution of neuron firing

The maze was linearized and divided into equal segments (bin size = 4.5 cm). Then firing rate vectors over respective bins were computed using a kernel based method. The firing rate was estimated at each bin x as: $f(x) = \Sigma(n_t * K(|x\text{-}x_t|) / \Sigma(dt * K(|x\text{-}x_t|))$, where n_t is the number of action potentials emitted in a given bin, dt is the amount of time spent in the bin, and K is the smoothing Gaussian kernel function (4.5 cm). The firing vector of each neuron was then z-transformed, and these were averaged together to derive the population responses.

Monte Carlo bootstrap analyses

This method[102] was selected since it requires no assumptions about the underlying distribution of the data and provides greater spatial resolution than comparable approaches. It tested the statistical significance of the firing rate differences of individual neurons between VD1, VD2 and SD task conditions in the sessions ($p < 0.0166$ with Bonferroni correction) as well as the differences ($p < 0.05$) between right versus left reward arm choice trials (called “side” selectivity) and rewarded versus non-rewarded trials (called “reward” selectivity). (Of course, SD trials could not be compared for right versus left choices.) Let us take as an example testing for differences in firing rate between two series of trials when the rat performed at criterion levels the VD task the first time versus the SD task. For each neuron, the average firing rate F was calculated at each bin x for each condition and the difference was taken: $D(x) = F_{SD}(x)\text{-}F_{VD1}(x)$. To test the statistical significance of the rate differences D(x) with the bootstrap procedure, the distribution of possible rate differences Dr(x) is estimated by randomly permuting the identity of each trial into proxy groups $F'_{SD}(x)$ and $F'_{VD1}(x)$. This process was repeated 5000 times to obtain the distribution from the resampled data, Dr1(x),..., Drn(x). With this shuffled dataset, the pointwise confidence limits (demarcating the upper and lower 2.5% of the distributions) were computed for each bin x. To deal with multiple comparison issues, the method also computes the global 5% bands. A maze zone (i.e., contiguous series of spatial bins) is considered to have significant different firing only when D(x) crosses both the global and pointwise bands, and the zone extent is determined only by the points where D(x) lies beyond the pointwise band. To test for behavioral correlates in assemblies or neurons (task condition, rewarded versus non-rewarded trials, etc.) the Monte Carlo bootstrap test had to be significant for at least one bin of the maze. This is referred to in a condensed manner as “spatial selectivity”, even though the respective segments of the maze correspond to different behavioral and cognitive aspects of the task .

Slope correction

To correct for gradual upward or downward drifts in assembly activations (or neuron firing rates) over the course of the recording sessions, a linear regression computed each assembly average activation (or neuron’s average firing rate) for each trial as a function of trial number (excluding the VD1, SD and VD2 criterion performance trials). The assembly or neurons with significant regressions (Spearman correlation $p < 0.05$, n = 11 assemblies, n = 105 neurons) were corrected by calculating the slope and subtracting the product of the (trial number minus 1) and the slope from the rate for each trial for the neuron. In a second approach, assemblies and neurons with significant regressions were simply discarded (rather than corrected). Since the two approaches gave similar result for the subsequent analyses, the slope corrected data is only presented in Figures S4A, S4C, and S4D.

Support Vector Machine analysis

With the libSVM library (https://www.csie.ntu.edu.tw/~cjlin/libsvm), support vector machines (SVMs) with RBF (radial basis function) kernel quantified how well STR or PFC population activity distinguished between trials in different pairs of trial conditions, namely VD1 versus SD, VD1 versus VD2, and VD2 versus SD. Each neuron's firing rate was averaged over each trial in a given task condition to obtain a population vector of length N, with N corresponding to the number of cells recorded during the session. Population vectors were z-scored in order to prevent neurons with high firing rates from having excessive influence on classification. Population vectors were then normalized by setting their euclidean norm to 1.

First, data were split in two balanced sets (e.g., 4 VD1 trials and 4 VD2 trials in each set). The first set was used to find optimal SVM hyperparameters γ and C, with γ as the exponent of a radial basis function kernel and C, the penalty parameter of the error term. We searched in a grid of values between 0.01 and 30 to find (C, γ) values that optimized a leave-one-out cross-validation accuracy. The accuracy of the SVM, i.e., its ability to correctly predict the epoch of the single left-out trial, was quantified. This procedure was iterated on each possible permutation (n = 8) of the dataset and for each pair (C, γ). The parameters with the best average cross-validation accuracy in each session were retained for subsequent analyses. With the second dataset, SVM were fit similarly using a leave-one-out cross validation procedure but with fixed hyperparameters (C, γ). To build a null distribution of prediction accuracy, the population activity vectors for each trial in each task condition were randomly assigned to one of the task conditions being compared. SVMs were then re-computed from these randomized datasets using again the first half of the dataset for setting hyper-parameters and the second half to compute SVM accuracies. We repeated this procedure 500 times. The actual prediction accuracy distributions (from second set) were then compared to the null distributions with the Wilcoxon rank-sum test.

Comparison of behavioral correlates of assemblies versus their members lacking significance for the correlate

The aim here was to determine, when the assembly showed a behavioral correlate in a part of the maze, whether those members lacking significance for this correlate there (in the Monte Carlo bootstrap analyses) nevertheless had a sub-significant tendency for the correlate anyway. (For this analysis, members were excluded if their significant behavioral correlate was in maze positions overlapping with the same correlate in the assembly.) For each member, we computed z-scores of the difference in each member's firing rate for the two trial characteristics (e.g., VD1 versus VD2, rewarded versus unrewarded, leftward versus rightward choice), but only in that part of the maze where the assembly had a behavioral correlate. For spatially selective activity, the z-score was taken relative to the mean firing rate. The signs of these z-score differences were rectified to correspond to the sign of the change of activation of the assembly. In this way, positive values would show tendencies toward the same response as the assembly. To provide a benchmark randomized distribution, z-score differences were again computed, but with activity of members at randomly selected locations on the maze (maintaining the same number of bins as for the initial distribution). A Wilcoxon signed rank test assessed if the differences between the median of the surrogate distribution and the true distribution were significantly different. This procedure was repeated for each behavioral correlate of each assembly.